MEASUREMENT OF HO_2 AND OTHER TRACE GASES IN THE STRATOSPHERE USING A HIGH RESOLUTION FAR-INFRARED SPECTROMETER

NASA GRANT NSG 5175

Annual Status Report No. 34

For the period 1 January 1994 to 31 December 1994

Principal Investigators

Wesley A. Traub
Kelley V. Chance

January 1995

Prepared for

National Aeronautics and Space Administration

Greenbelt, Maryland 20771

Smithsonian Institution
Astrophysical Observatory
Cambridge, Massachusetts 02138

The Smithsonian Astrophysical Observatory is a member of the Harvard-Smithsonian Center for Astrophsysics

The NASA Technical officer for this grant is Dr. William S. Heaps, Code 916, Atmospheric Experiments Branch, Goddard Space Flight Center, Greenbelt, Maryland 20771

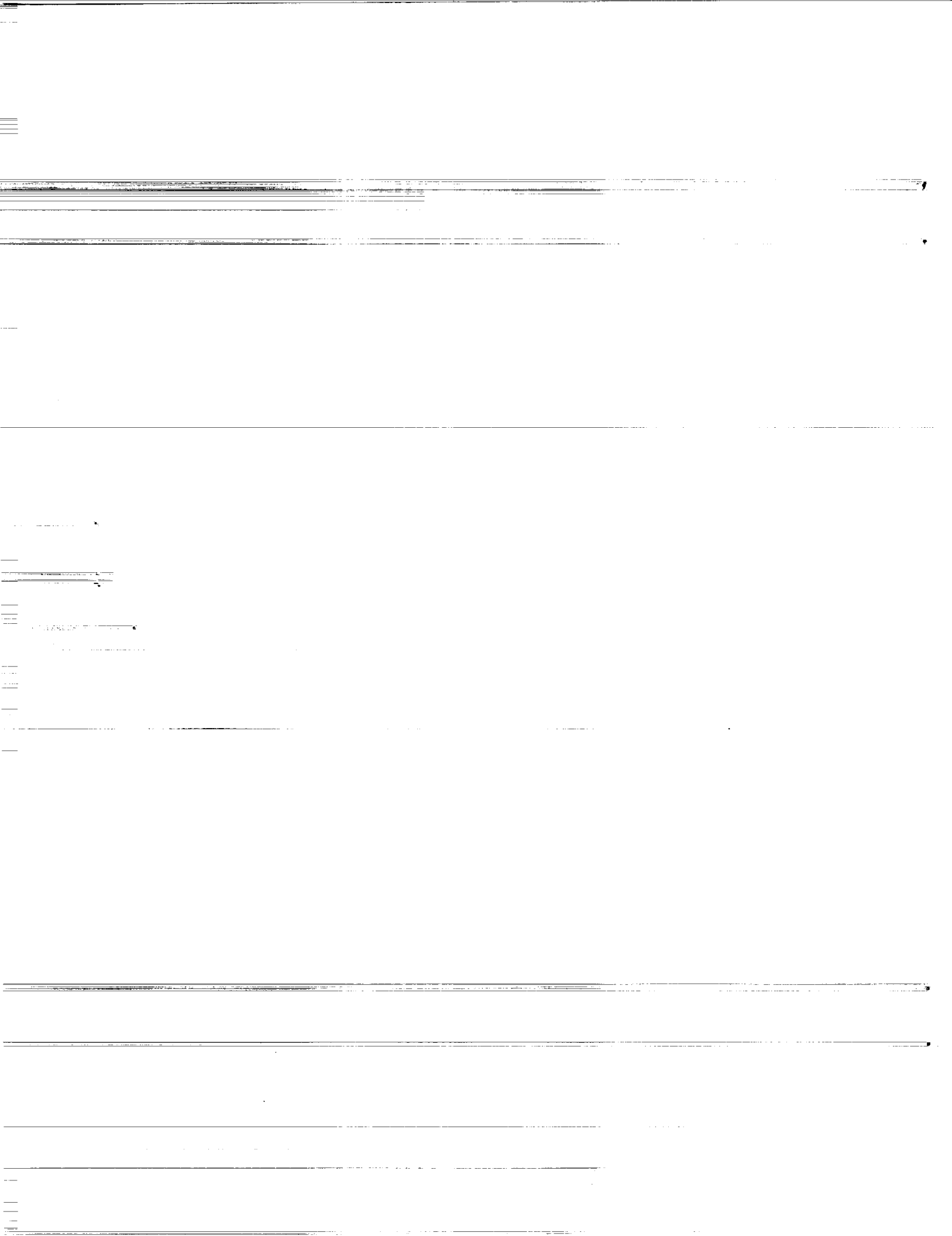

Annual Report No. 34

NASA Grant NSG-5175

Measurement of HO_2 and Other Trace Gases in the Stratosphere Using a High Resolution Far-Infrared Spectrometer

1. Personnel Working Under this Grant During this Reporting Period

Dr. Wesley A. Traub (Principal Investigator)

Dr. Kelly V. Chance (Principal Investigator)

Dr. David G. Johnson (Co-Investigator)

Dr. Kenneth W. Jucks (Co-Investigator)

Dr. Ross J. Salawitch (Co-Investigator)

Dr. Changqin (Jim) Xue (Programmer-Analyst)

Ms. Paola Ciarpallini (SAO Predoctoral Fellow)

2. Status Summary

This report covers the time period 1 January 1994 to 31 December 1994. During this reporting period we had our fourth Upper Atmosphere Research Satellite (UARS) correlative balloon flight; the data from this flight have been reduced and submitted to the UARS CDHF. We have spent most of the past year analyzing data from this and past flights. For example, using data from our September 1989 balloon flight we have demonstrated for the first time ever that the rates of production and loss of ozone are in balance in the upper stratosphere. As part of this analysis, we have completed the most detailed study to date of radical partitioning throughout the stratosphere. We have also produced the first measurements of HBr and HOBr mixing ratio profiles over a full diurnal cycle.

3. AASE II

We completed two papers discussing results from the second Airborne Arctic Stratospheric Expedition (AASE II), both of which appeared in Geophysical Research Letters during this reporting period. The paper "Comparison of Column Abundances from Three Infrared Spectrometers During AASE II" (included as Appendix A) presents a detailed comparison of the measurements of HF, HCl, O_3, HNO_3, and H_2O made by the three Fourier transform infrared spectrometers (SAO, NCAR, and JPL instruments) on the DC-8 during AASE II. The measurements made by the three different groups are in excellent agreement. The paper "Chemical Change in the Arctic Vortex During AASE II" (included as Appendix B) presents a preliminary analysis of the changes in the observed column densities of HCl, O_3, HNO_3, and H_2O inside the Arctic vortex. We correct the columns for the effects of subsidence, so that the remaining changes reveal chemical processing.

4. UARS Correlative Measurements Program

We had our fourth UARS correlative flight (and ninth flight overall) during this reporting period. The balloon was launched from Ft. Sumner, New Mexico at 8:30 AM MDT on May 22, 1994, and reached the float altitude of 122,000 feet at 10:45 AM. The balloon was terminated near the New Mexico-Arizona border at 8:45 AM on May 23, achieving 22 hours at float. We have

completed the data reduction for this flight, and the results have been submitted to the UARS CDHF.

The gondola for this flight carried the JPL MKIV interferometer and in-situ ozone instrument in addition to the SAO spectrometer. SAO and JPL measure many of the same molecules, and we have begun to compare profiles for the overlapping species. The early results show that our measured profiles are in excellent agreement. We look forward to using the large combined data set for detailed testing of the results of photochemical models.

In preparation for our latest balloon flight we made several improvements to the instrument. First, we replaced our vintage 1985 power supplies with newer and more efficient DC-DC converters. As measured during the 1994 flight, use of the new converters has reduced the flight instrument power consumption by 44%, which reduces our battery requirement by almost a factor of 2. Second, we have installed a new Mylar beamsplitter which is roughly 5% thicker than the old one. Using a thicker beamsplitter has increased the signal to noise ratio in the region 540–600 cm^{-1} by up to a factor of 10, which will improve our retrievals of N_2O and CO_2 (CO_2 lines in this region are used to correct the pointing angles). We are also searching this region for spectral features of N_2O_5 and $ClNO_3$, with the hope of eventually retrieving mixing ratio profiles for these species.

5. Analysis of Balloon Flight Data

We have completed a new analysis of data from the May 1988 FIRS-2 balloon flight which was begun during the last reporting period. We have also completed some software modifications which will make it possible to use our current algorithms to process the data from flights of the FIRS-1 instrument (1977–1983). We will proceed with the analysis of old data sets as time permits.

We have compared the results of our retrieval algorithms with results presented by 16 other groups as part of the European Stratospheric Monitoring Stations/Network for the Detection of Stratospheric Change (ESMOSII/NDSC) algorithm intercomparison exercise. It was gratifying for us to find that our results are consistent with the results obtained by the majority of the participants.

By combining data from 7 balloon flights we produced daytime and nighttime profiles for HBr and HOBr with precisions of 1.3 and 5 ppt, respectively. A paper describing this analysis has been submitted to the Journal of Geophysical Research (JGR), and is included as Appendix C. This is the first measurement of HOBr that we are aware of, and the simultaneous measurements of HBr and HOBr through a full diurnal cycle will be useful in testing models of the stratospheric photochemistry of bromine.

6. Chemical Modeling

As part of our ongoing analysis of the FIRS-2 data set we have developed a method of estimating the abundance of ClO from FIRS measurements of HO_2, OH, and HOCl; a paper comparing calculated and measured ClO for a balloon flight in September 1992 has been submitted to JGR and is included as Appendix D.

We are also continuing the analysis of radical chemistry outlined in the last semiannual report, and have two manuscripts in preparation. The first paper, which has been submitted to JGR and is included as Appendix E, presents a detailed comparison of hydrogen, chlorine, and nitrogen species (both radicals and reservoirs) with results from a photochemical model. In a second manuscript in preparation, we extend this analysis and use our measurements to calculate rates of production and loss of ozone throughout the stratosphere; preliminary results from this analysis are presented in Figures 1 and 2. The important conclusions which can be drawn from these figures are that ozone production and loss rates are in balance in the middle stratosphere (25–40 km) where the photochemical lifetime of ozone is short compared to the characteristic transport time, and that

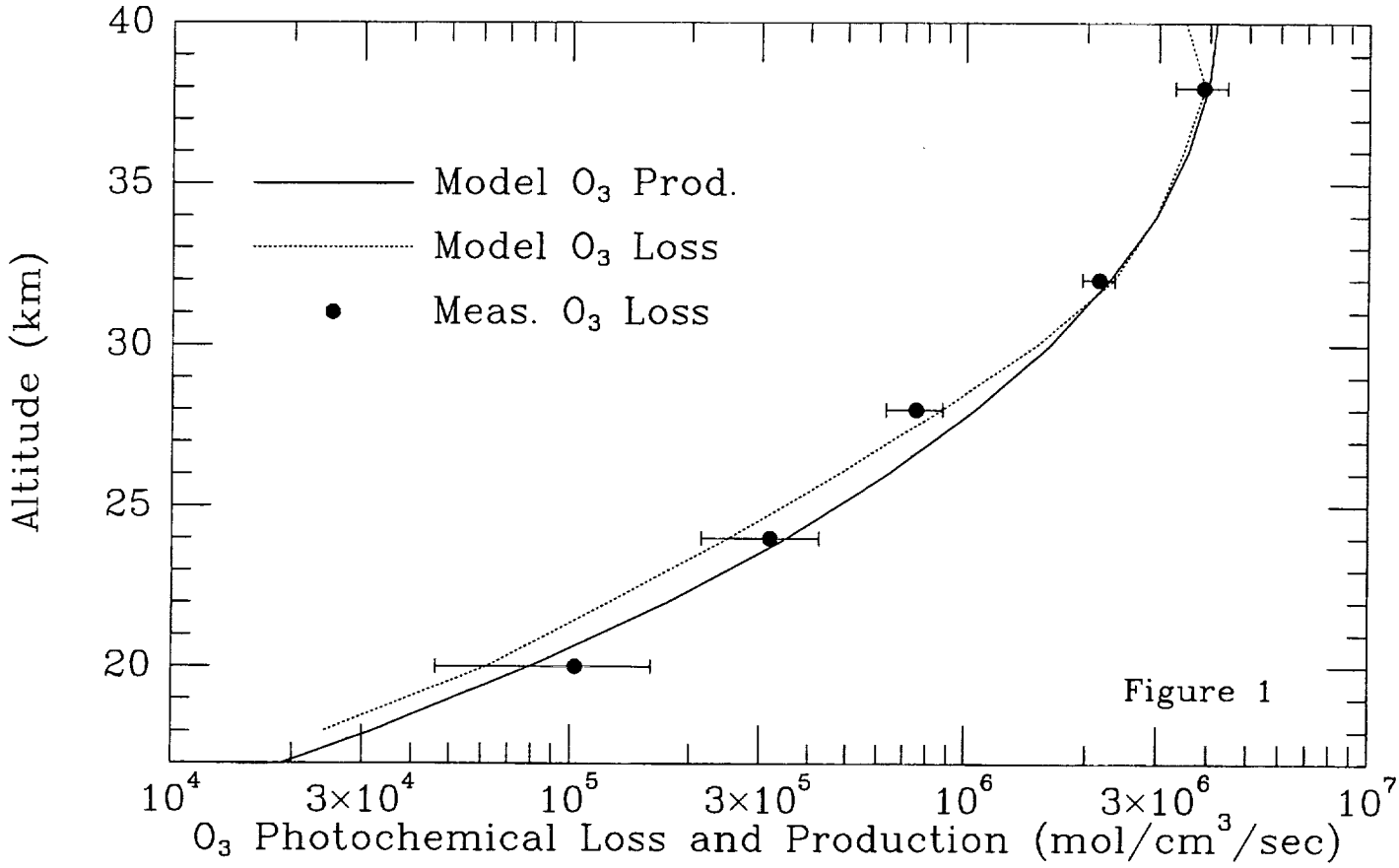

Figure 1

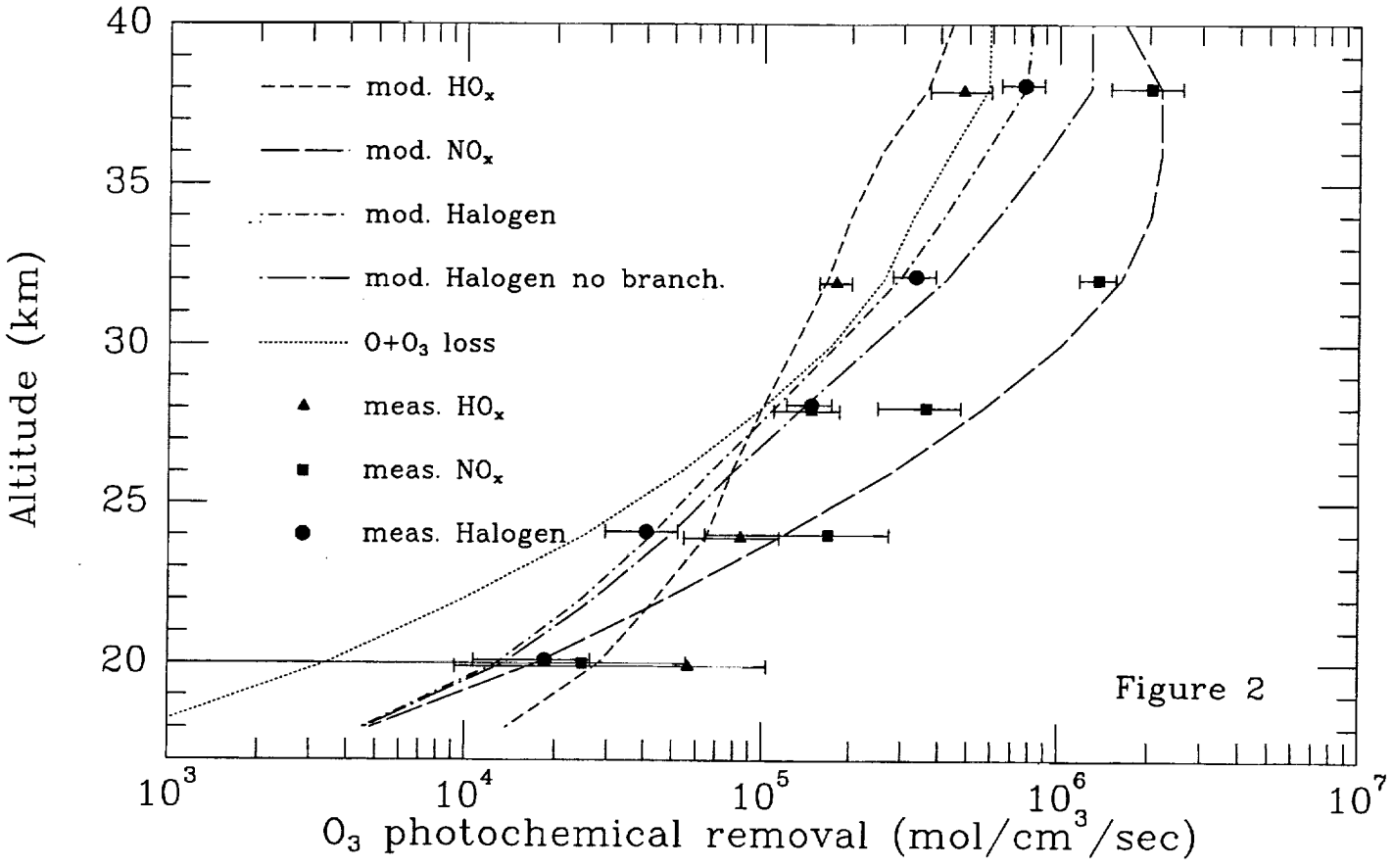

Figure 2

the NO_X cycles dominate ozone destruction in most of the stratosphere. The latter conclusion has implications for estimating the impact of a fleet of stratospheric aircraft on the ozone layer.

7. Publications and Presentations

W. A. Traub, K. W. Jucks, D. G. Johnson, M. T. Coffey, W. G. Mankin, and G. C. Toon, Comparison of Column Abundances from Three Infrared Spectrometers During AASE II, *Geophysical Research Letters 21*, 2591–2594, 1994.

W. A. Traub, K. W. Jucks, D. G. Johnson, and K. V. Chance, Chemical Change in the Arctic Vortex During AASE II, *Geophysical Research Letters 21*, 2595–2598, 1994.

K. V. Chance, K. W. Jucks, D. G. Johnson, and W. A. Traub, The Smithsonian Astrophysical Observatory database SAO92, *J. Quant. Spectrosc. Radiat. Transfer 52*, 445–457, 1994.

D. G. Johnson, K. W. Jucks, W. A. Traub, and K. V. Chance, The Smithsonian Stratospheric Far-Infrared Spectrometer and Data Reduction System, accepted by JGR, 1994.

D. G. Johnson, W. A. Traub, K. V. Chance, K. W. Jucks, and R. A. Stachnik, Estimating the Abundance of ClO from Simultaneous Remote Sensing Measurements of HO_2, OH, and HOCl, submitted to JGR.

D. G. Johnson, W. A. Traub, K. V. Chance, and K. W. Jucks, Remote Sensing Measurements of HBr and HOBr and Implications for Bromine Partitioning in the Stratosphere, submitted to JGR.

K. Chance, W. A. Traub, D. G. Johnson, K. W. Jucks, P. Ciarpallini, R. A. Stachnik, R. J. Salawitch, and H. A. Michelsen, Simultaneous Measurements of Stratospheric HO_X, NO_X, and Cl_X: Comparison with a Photochemical Model, submitted to JGR.

APPENDIX A

Comparison of Column Abundances from Three Infrared Spectrometers During AASE II

GEOPHYSICAL RESEARCH LETTERS, VOL. 21, NO. 23, PAGES 2591-2594, NOVEMBER 15, 1994

Comparison of column abundances from three infrared spectrometers during AASE II

W. A. Traub. K. W. Jucks and D. G. Johnson
Smithsonian Astrophysical Observatory, Cambridge, Massachusetts

M. T. Coffey and W. G. Mankin
National Center for Atmospheric Research, Boulder, Colorodo

G. C. Toon
Jet Propulsion Laboratory, Pasadena, California

Abstract. Three Fourier transform infrared (FTIR) spectrometers were on board the NASA DC-8 during the second Airborne Arctic Stratospheric Expedition (AASE II) in 1992. Two FTIRs used solar absorption and one used thermal emission. We compare over 2000 measurements from these 3 FTIRs, on 12 DC-8 flights, for closely coincident air masses and times, both inside and outside the polar vortex. In the majority of cases the offset biases are quite small, in the range 1-4%, and comparable to the absolute precisions expected. In most cases the rms scatter is in the range 4-11%; this scatter is unlikely to be geophysical, but rather is probably instrumental or analytical in origin.

Introduction

In this paper we compare results from the 3 FTIR spectrometers on board the NASA DC-8 during the AASE II campaign in 1992. The overall scientific goals of the AASE II campaign [*Anderson and Toon*, 1993] were to investigate both the potential for ozone loss in the Arctic during the coming decade, and contemporary ozone loss at northern mid-latitudes. A suite of 13 instruments was therefore assembled to make measurements.

Instruments

SAO FTIR

This spectrometer, also called the far-infrared spectrometer (FIRS-2), was built at the Smithsonian Astrophysical Observatory (SAO), and has flown on 9 balloon flights from 1987 through 1994, plus 19 DC-8 flights for AASE II. The instrument, data analysis, and calibration are discussed in *Traub et al.* [1991, 1994], *Abbas and Traub* [1992], and *Johnson et al.* [1994]. The SAO FTIR simultaneously measures in the far-infrared (80–200 cm^{-1}) with apodized resolution 0.008 cm^{-1}, and, on these flights, 0.024 cm^{-1} in the mid-infrared (350–700 cm^{-1}). The instrument measures a thermal emission spectrum. The atmosphere is viewed at 7 elevation angles from 0°to 32°(corrected for aircraft roll angle), plus 2 calibration scans, in an 11-min cycle. The viewing azimuth is +90°from the aircraft heading, i.e., through a right (starboard) side window opening.

For each species, from 1 to 17 microwindows are selected, and a least-squares spectral-line fitting analysis is done. Initial volume mixing ratio (*vmr*) profiles are taken from standard mid-latitude ATMOS results, with the secularly-increasing species (HF and HCl) updated to 1992. Temperature and pressure profiles are from National Meteorological Center (NMC) data, for the time and location of the DC-8.

In each observing sequence, HF is analyzed first, by allowing the initial HF profile (vmr_0) to be scaled vertically, to model the effect of subsidence, using the simple law $vmr(z) = vmr_0[(1+s)z]$, where s is the (dimensionless) subsidence factor [*Toon et al.*, 1992]. Estimated subsidences from each of the upper 4 elevation angles are combined to form a weighted mean. This is then used for the analysis of all other species in the same observing sequence. For these other species, the subsided model profiles are scaled in amplitude. The purpose of this two-step model process is to separate the effects of dynamics and chemistry.

JPL FTIR

The JPL spectrometer, also called the MkIV interferometer, was designed and built at the Jet Propulsion Laboratory (JPL). It has operated on the ground at McMurdo Station in 1986; on the DC-8 in 1987, 1989, and 1992; and has performed 7 successful balloon flights from 1989 through 1994. The instrument and data reduction technique are described in *Toon et al.* [1989, 1991, 1992]. The entire 650 to 5450 cm^{-1} spectral range is measured simultaneously at an apodized resolution of 0.02 cm^{-1} on the DC-8. One spectrum is recorded every 50 sec. The instrument measures the solar spectrum from the center of the disc, with atmospheric absorption superposed. The DC-8 is typically flown on a path which keeps the solar elevation angle in an optimum range (2 to 5°) as long as possible (1 to 2 hr.). A sun tracker is used for elevation and azimuth pointing correction. The viewing azimuth is −85 to −95° from the aircraft heading, i.e., out the left (port) side.

Spectra are averaged in groups of 5 to 15; up to 15 microwindows per species are analyzed using least-squares spectral-line fitting. Initial model *vmr* profiles are from standard mid-latitude ATMOS results, with HF and HCl updated to 1992. Analyses are performed using 2 atmospheric temperature/pressure profiles, one for warm mid-latitudes and one for a cold high latitudes.

Paper number 94GL01173
0094-8534/94/94GL-01173$03.00

The actual atmosphere used is a linear interpolation between these two using the NMC temperature at the time and location of the measurement.

For the AASE II flights, HF is analyzed first, not by scaling the amplitude of the *vmr* profile, but by allowing the profile to be compressed vertically, using the subsidence relation given above. For other species, the subsided profiles are scaled in amplitude. In these respects, the JPL and SAO procedures are the same.

NCAR FTIR

This spectrometer was built by the National Center for Atmospheric Research (NCAR) around an Ecom modulator and has flown on over 200 flights of the NCAR Saberliner, NASA P3, Electra and DC-8 aircraft from 1978 through 1993. The instrument and data acquisition are discussed in *Mankin* [1978], *Mankin and Coffey* [1989], *Coffey et al.* [1989], and *Mankin et al.* [1990]. The spectral range is 700 to 5000 cm^{-1}; the apodized resolution is 0.06 cm^{-1}. Each spectrum requires 6 sec to record. The instrument measures solar emission and atmospheric absorption, and uses a sun tracker in an elevation range -2 to 15°. The viewing azimuth is -75 to -105° from the aircraft heading, i.e., the left (port) side.

Spectra are averaged in groups of 10, and 1 to 4 spectral regions per species are used. Data analysis methods are noted in *Gaines et al.* [1993]. Briefly, for HF and HCl an equivalent width method is used, such that the depth of the target absorption feature is measured, and the corresponding line of sight column abundance is determined using a precomputed curve of growth. For O_3 and HNO_3 a least-squares spectral line fitting program (SFIT) is used [*Rinsland et al.*, 1982]; for H_2O an interactive method is used to adjust a calculated spectrum to match the observed spectrum.

The model *vmr* profiles for HF, HCl and HNO_3 are mid-latitude ones from *Coffey et al.* [1989]; O_3 is from *Mankin and Coffey* [1989]; H_2O is from *Smith* [1982], lowered by 4 km in the Arctic; temperature and pressure are from *Barnett and Corney* [1985]. The columns reported in the AASE-II CD-ROM are vertical integrals above the aircraft altitude, except for H_2O which is reported as the integrated column above 200 mb; for H_2O the values reported here differ from the CD-ROM in that they are columns above the aircraft.

For all species, the adjustable parameter is the *vmr* amplitude scaling factor. In particular, except for the 4 km offset for H_2O mentioned just above, the profiles are not adjusted vertically.

Comparison Method

To compare results from the SAO, JPL, and NCAR FTIRs, we compiled all overlap species during all common measurement periods. The data are displayed in Fig. 1. The overlap species are HF, HCl, O_3, HNO_3, and H_2O. With the single exception of NCAR H_2O, all the data presented here have already been published in the AASE II CD-ROM [*Gaines et al.*, 1993]. The 1992 UT date at the beginning of each flight, and the length of each common observing period (in 10^3 sec) is as follows: January 14(8), 16(3), 19(12.5), 22(16); February 17(9), 20(5.5), 22(14); March 10(7.5), 12(6.5), 14(8.5), 18(11), and 20(8). The number of observations used are SAO, 690; JPL, 615; and NCAR 732. The totals are 2037 observations over 30.4 hours.

All of the observations in Fig. 1 were carried out between the latitudes of 50 and 84°N, and longitudes from 20°E to 140°W, except for the February 20 run at about 20°N and 67°W near Puerto Rico. Observations were made both inside the Arctic vortex (characterized by large HF columns) and outside the vortex (small HF columns). This wide range of conditions gives rise to a correspondingly large dynamic range in column abundances, with a factor of about 4 for HF and HCl, a factor of 3 for O_3, and a factor of about 2 for HNO_3 and H_2O. The 3 FTIRs track these dynamic swings quite well, with few exceptions.

In each panel in Fig. 1, we determine a time series of median values by computing the median of all data points in a sliding window of width 3000 sec. If there are fewer than 5 points in any window, the width is increased until this threshhold is reached. The resulting time series is then fit with a cubic polynomial (lower order in the shortest 2 panels). The resulting curve follows closely the one that might be drawn by eye.

Comparison Statistics

We define the relative deviation of a measurement as

$$\text{relative deviation} = (\text{data} - \text{median})/\text{median},$$

where "median" refers to the smooth median trend line at the time of the data point. For each instrument and species combination we calculate the relative deviation of each data point; we define the offset bias to be the average of these values, for all 12 flights together. The offset bias values are collected in Table 1; a positive offset means that the value exceeds the median.

We also calculate a root-mean-square (rms) deviation for each instrument and species combination. This rms is defined as the square root of the average of the squares of the difference between each data point and the median-plus-single-flight offset bias. The rms values are collected in Table 2.

Discussion

From Table 1 we see that the offsets fall in 2 groups. In the first group, with 67% (10/15) of the entries, the offsets are small, in the range 1–4%. This is typical of what might be expected from systematic errors in spectroscopic parameters, zero levels, or gains.

The species HCl and O_3 show offset biases of 1–3%. Since it is unlikely that biases this small would occur by chance, we suggest that this represents an estimate of the true inter-instrumental differences. (Note that the biases (e.g., HCl) do not have to sum to zero, as they are measured with respect to a median, not an average.)

The remaining biases are larger, in the range 6–13%. We briefly consider each of these.

The SAO HF columns are about 12% larger the median, which could be caused by either a line-broadening parameter which is too small (since the HF line is saturated), or the fact that the SAO instrument always viewed a more polar airmass than the others. To test the latter hypothesis, we used potential vorticity (PV) maps to determine the difference in effective PV seen across a span of 170 km (50 km to starboard plus 120 km to port), and a measure of the empirical gradient at a typical vortex wall point [*Traub et al.*, 1994]; we found that the SAO HF should tend to be about 2%

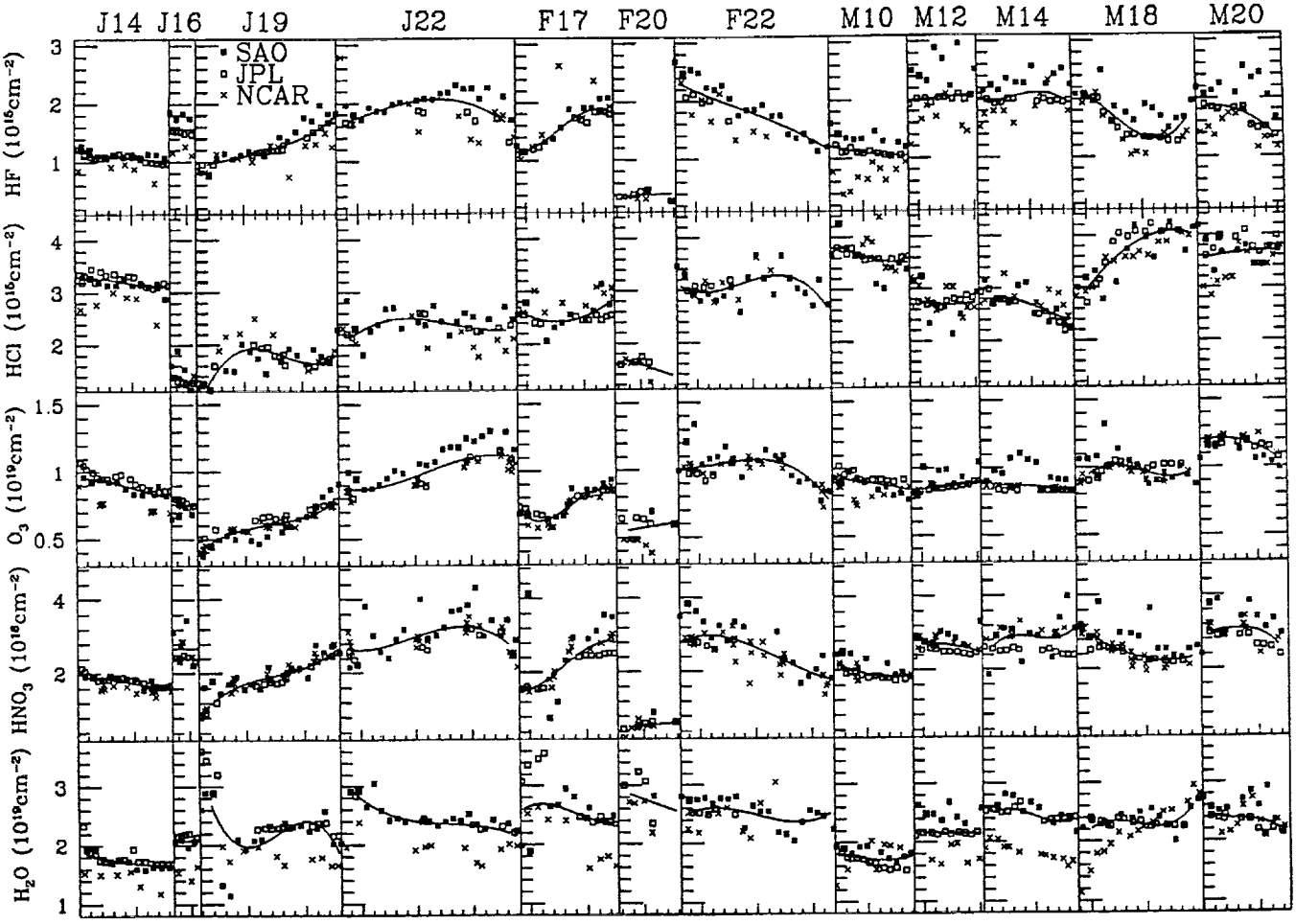

Figure 1. Column abundances of HF, HCl, O_3, HNO_3, and H_2O, during the AASE II campaign in January, February, and March 1992, as measured on the DC-8 by 3 FTIRs: SAO (solid square), JPL (open square), and NCAR (4-point star). Abscissa tics are 1000 sec. The smooth line in each panel is the median trend.

larger than the other instruments, which is insufficient to explain the observed difference.

The SAO HNO_3 column is about 9% above the median, which could be due to causes similar to those for HF, but in this case there is an additional factor of relatively high scatter due to reduced signal-to-noise in this channel, which may make the absolute calibration correspondingly uncertain.

There is an 11% difference on average between the NCAR and JPL columns of HF, with NCAR giving the smaller values. Both of these instruments have essentially the same line of sight and air mass, and use the same spectral line. Differences in analysis are the most likely cause of the offset. In particular, differences in treatment of the profile may contribute much of the discrepancy: JPL squashes its profile vertically, whereas NCAR multiplies its profile by a constant at all altitudes. In a previous (unpublished) comparison of JPL and NCAR spectra from a 1989 AASE I DC-8 flight, it was found that the bias was substantially reduced when a single analysis package was used, clearly indicating that analytical methods can be an important source of bias.

The NCAR H_2O column is about 16% smaller than the SAO and JPL values. Since the aircraft often flew close to the hydropause, we sometimes had tropospheric water in our line of sight. The water *vmr* has a very steep vertical gradient below the hydropause. It is possible that differences in modeling this component are the cause of part of the bias.

Inspection of Fig. 1 and Table 1 together shows that the biases are not the same from day to day. We have no explanation for this drift.

Table 1. Offset bias: FTIRs on DC-8 (12 flights)

Species	SAO (%)	JPL (%)	NCAR (%)
HF	12	−2	−13
HCl	1	1	1
O_3	3	2	− 3
HNO_3	9	−6	− 2
H_2O	4	4	−12

Table 2. RMS deviation: FTIRs on DC-8 (12 flights)

Species	SAO (%)	JPL (%)	NCAR (%)
HF	10	4	16
HCl	11	7	11
O_3	8	4	5
HNO_3	21	5	9
H_2O	9	7	11

APPENDIX B

Chemical Change in the Arctic Vortex During AASE II

The rms scatter entries in Table 2 show that in 13 of 15 cases (87%) the rms is in the range 4–11%. The 2 other cases are the relatively large values for the SAO HNO_3, which was noted above as being in a low signal-to-noise band during these flights, and the NCAR HF, which tends to have significant outlier points.

For AASE I, *Toon et al.* [1992] showed that derived abundance variations due to geophysical fluctuations were small compared to the measurement precision; thus 50-sec observations were averaged in larger groups with little loss of information. (Inspection of Fig. 2 in *Toon et al.* [1992] shows that the rms scatter in AASE I was comparable to that in AASE II, so the 2 JPL data sets can be compared.) This suggests that the rms deviations in Table 2 are not atmospheric in origin.

Conclusion

We compared the results of 3 FTIR instruments on the DC-8, measuring 5 species in common over a period of about 30 hours, distributed over 12 flights during the AASE II campaign. The meteorlogical conditions varied significantly, from inside the polar vortex to well outside. The columns of each species varied dramatically, by factors of 2 to 4. We removed the dominant trend in column abundance for each day by subtracting a smooth median from the individual observations. In the majority of cases the systematic offsets are quite small, 1–4%. The rms scatter exceeds the atmospheric variation, and is probably due to instrumental or analytical effects. Overall, the comparison shows that there is a large degree of agreement between the instruments, but that improvements might yet be made in some areas.

The present paper is limited to comparing results which were obtained and analyzed independently by 3 groups. In future comparisons, it might be worthwhile having more communication between groups at an earlier stage to minimize systematic differences in modeling. With this caveat, it is hard to imagine a better set of conditions for comparison than existed on these flights.

Acknowledgments. The work at SAO was supported by NASA grant NSG-5175. Part of this research was performed at the Jet Propulsion Laboratory, California Institute of Technology, under contract with NASA. The work at NCAR was partially supported by NASA through W-18143; NCAR is supported by the National Science Foundation. The authors are grateful for assistance from the NASA Ames DC-8 flight and ground crews throughout the AASE II mission.

References

Abbas, M. and W. A. Traub, Stratospheric minor constituent distributions from far-infrared thermal emission spectra, *J. Geophys. Res., 97,* 18035-18045, 1992.

Anderson, J. G., and O. B. Toon, Airborne arctic stratospheric expedition II: an overview, *Geophys. Res. Lett., 20,* 2499-2502, 1993.

Barnett, J. J. and M. Corney, Middle atmosphere reference model derived from satellite data, *Handbook for MAP, 16,* 47-85, University of Illinois, 1985.

Coffey, M. T., W. G. Mankin, and A. Goldman, Airborne measurements of stratospheric constituents over Antarctica in the austral spring 1987, 2. halogen and nitrogen trace gases, *J. Geophys. Res., 94,* 16597-16613, 1989.

Gaines, S., P. Hathaway, and S. Hipskind, eds., AASE II CD-ROM, NASA/UARP-004, Edition 2, NASA Ames Research Center, 1993.

Johnson, D. G., K. W. Jucks, W. A. Traub, and K. V. Chance, The Smithsonian stratospheric far-infrared spectrometer and data reduction system, *submitted to J. Geophys. Res.,* 1994.

Mankin, W. G., Airborne Fourier transform spectroscopy of the upper atmosphere, *Opt. Eng., 17,* 39-43, 1978.

Mankin, W. G. and M. T. Coffey, Airborne measurements of stratospheric constituents over Antarctica in the austral spring 1987, 1. Method and ozone observations, *J. Geophys. Res., 94,* 11413-11421, 1989.

Mankin, W. G., M. T. Coffey, A. Goldman, M. R. Schoeberl, L. R. Lait, and P. A. Newman, Airborne measurements of stratospheric constituents over the Arctic in the winter of 1989, *Geophys. Res. Lett., 17,* 473-476, 1990.

Rinsland, C. P., A. Goldman, F. J. Murcray, D. G. Murcray, M. A. H. Smith, R. K. Seals, Jr., J. C. Larsen, and P. L. Rinsland, Stratospheric N_2O mixing ratio profile from high-resolution balloon-borne solar absorption spectra and laboratory spectra near 1880 cm-1, *Appl. Opt., 21,* 4351-4355, 1982.

Smith, M. A. H., Compilation of atmospheric gas concentration profiles from 0 to 50 km, NASA TM 83289, 1982.

Toon, G. C., C. B. Farmer, L. L. Lowes, P. W. Schaper, J.-F. Blavier and R. H. Norton, Infrared aircraft measurements of stratospheric composition over Antarctica during September 1987, *J. Geophys. Res., 94,* 16571-16596, 1989.

Toon, G. C., The JPL MkIV interferometer, *Optics and Photonics News, 2,* 19-21, 1991.

Toon, G. C., C. B. Farmer, P. W. Schaper, L. L. Lowes, and R. H. Norton, Composition measurements of the 1989 arctic winter stratosphere by airborne infrared solar absorption spectroscopy, *J. Geophys. Res., 97,* 7939-7961, 1992.

Traub, W. A., K. V. Chance, D. G. Johnson, and K. W. Jucks, Stratospheric spectroscopy with the far-infrared spectrometer (FIRS-2): overview and recent results, *SPIE, 1491,* 298-307, 1991.

Traub, W. A., K. W. Jucks, D. G. Johnson, and K. V. Chance, Subsidence of the Arctic stratosphere determined from thermal emission of HF, *submitted to J. Geophys. Res.,* 1994.

M. T. Coffey and W. G. Mankin, National Center for Atmospheric Research, P. O. Box 3000, Boulder, CO 80307; email: coffey@ncar.ucar.edu, mankin@ncar.ucar.edu

D. G. Johnson, K. W. Jucks, and W. A. Traub, Smithsonian Astrophysical Observatory, 60 Garden Street, Cambridge, MA 02138; email: dgj@cfa.harvard.edu, jucks@cfa.harvard.edu, traub@cfa.harvard.edu

G. C. Toon, Jet Propulsion Laboratory, 4800 Oak Grove Drive, Pasadena, CA 91109 email: toon@mark4sun.jpl.nasa.gov

(received March 14, 1994;
accepted May 4, 1994.)

GEOPHYSICAL RESEARCH LETTERS, VOL. 21, NO. 23, PAGES 2595-2598, NOVEMBER 15, 1994

Chemical change in the arctic vortex during AASE II

Wesley A. Traub, Kenneth W. Jucks,
David G. Johnson, and Kelly V. Chance
Smithsonian Astrophysical Observatory, Cambridge, Massachusetts

Abstract. We measured column abundances of HF, HCl, O_3, HNO_3, and H_2O on the NASA DC-8 during the AASE II campaign, using thermal emission spectroscopy. We made multiple traversals of the Arctic vortex and surroundings. Using HF as a tracer, we remove the effects of subsidence from the measured column abundances; perturbations in the resulting column abundances are attributed to chemical processing. We find that by January 1992 the stratospheric column in the vortex had been chemically depleted by about (55±10)% in HCl and (35±10)% in O_3, and enhanced by about (15±10)% in HNO_3 and (0±10)% in H_2O.

Introduction

A major goal of the second Airborne Arctic Stratospheric Expedition (AASE II) in 1991–92 was to quantify the effects of dynamics and chemistry during the Arctic winter. An overview of the campaign is found in *Anderson and Toon*, [1993]. As one of 13 experiments flown on the DC-8 during AASE II, the Smithsonian's far-infrared spectrometer (FIRS-2) measured column abundances using the thermal emission spectrum of the stratosphere, during both day and night. Here we report the results of our measurements of HCl, O_3, HNO_3, and H_2O, using HF as a tracer to remove the effects of subsidence and to infer chemical change.

The results from FIRS-2 are compared to those of 2 other Fourier-transform infrared spectrometers (FTIRs) on board the DC-8 in *Traub et al.*, [1994a]. The latter paper shows that the 3 FTIRs compare well with one another during the 30 hours of common-mode measurement; the majority of cases yield offset biases in the range 1–4%, and rms scatter values in the range 4–11%, thus validating the individual FTIRs within these limits.

Observations

The data reported here are from 13 DC-8 flights, with 102 hours of observation which yielded 7336 sky interferograms and 2096 calibration interferograms; the observing time per interferogram is 35 sec, plus an additional 4 sec overhead on the average. Each pair of 2 scans is Fourier-transformed, phase-corrected, and coadded to produce an individual spectrum. Each spectrum is analyzed separately, to preserve spatial resolution. The apodized spectral resolution is $0.008\,cm^{-1}$ in the far-infrared (80–200 cm^{-1}), and on these flights $0.024\,cm^{-1}$ in the mid-infrared (350–700 cm^{-1}).

In Fig. 1a we show an O_3 microwindow for a typical single spectrum. All spectra are intensity-referenced to a 277K blackbody. The signal-to-noise ratio (SNR) in Fig. 1a is characteristic of that found in other parts of the far-infrared, and on other flights. For O_3, HF, HCl, and H_2O the analysis is done at elevation angles of 32, 16, 8, and 4°; spectra at smaller angles are not used for these species, since the water-vapor continuum opacity becomes too strong. For illustration, we show in Figs. 1b–e the sum of 65 spectra in single microwindows for these 4 species and 4 elevation angles.

For HNO_3 the analysis is done at elevation angles of 4, 2, 1, and 0°; spectra at larger angles are not used because the lines are too weak. Fig. 1f shows a typical mid-infrared microwindow for HNO_3, again for the sum of 65 spectra. The mid-infrared continuum is relatively weak. In general, the mid-infrared SNR is smaller than in the far-infrared, owing to vibration in the spectrometer. The negative baseline in Fig. 1f is likely caused by the low SNR; the error analysis includes a contribution from the baseline uncertainty.

Data Analysis

Our analysis of FIRS-2 spectra is carried out in several stages. The basic reduction procedure is given in *Johnson et al.*, [1994]; only those aspects peculiar to AASE II are mentioned here. The first stage is to determine the degree of stratospheric subsidence, by measuring the column abundance of HF in each spectrum, and using the transformation $vmr(z) = vmr_0[(1+s)z]$. Here $vmr(z)$ is the volume mixing ratio profile, vmr_0 is a standard mid-latitude profile, and s is the (dimensionless) subsidence factor [*Toon et al.*, 1992a]. We vary s to make the calculated spectrum match the observed spectrum. This process is detailed in *Traub et al.* [1994b], where it is shown that (1) the measured degree of subsidence correlates well with Ertel's potential vorticity (PV), (2) this relationship evolves over the second half of the winter (January through March), and (3) the changes in subsidence with time can be used to estimate the average vertical velocity in the vortex (-0.052 ± 0.013 cm/s) during the winter. Subsidence is the dominant effect in the variation of observed column abundances in the Arctic [*Traub et al.*, 1994a], causing increases of about a factor of 4 for HF and HCl, 3 for O_3, and 2 for HNO_3 and H_2O. Therefore, the removal of the effects of subsidence paves the way for the determination of chemical change, which follows.

Paper number 94GL01324
0094-8534/94/94GL-01324$03.00

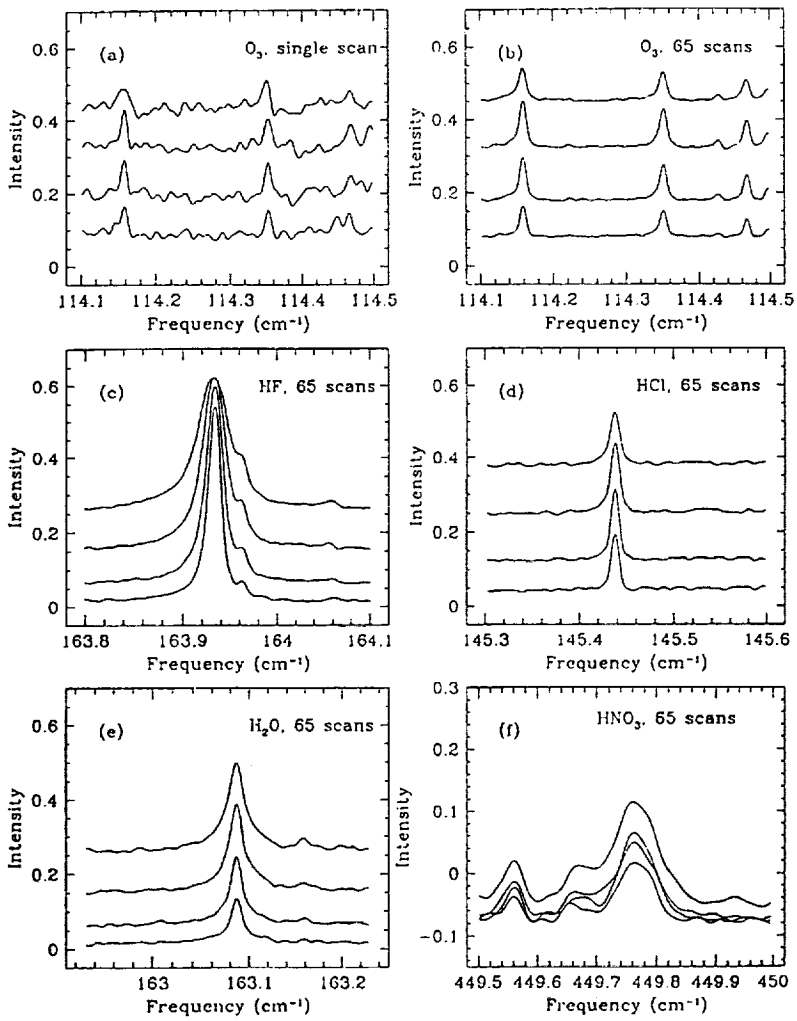

Figure 1. Sample microwindows for column abundance retrievals. The elevation angles in (a–e) are 32, 16, 8, and 4°; the angles in (f) are 4, 2, 1,and 0°.

In the second stage of the analysis, we apply the measured subsidence from HF to *vmr* profiles of other species. The subsided *vmr* profiles are scaled in amplitude so that the calculated spectra match the observed spectra. Details are given in *Johnson et al.* [1994]. This method assumes that: (1) stratospheric mixing ratio profiles are dependent only on subsidence and chemical change, i.e., independent of latitude, longitude, and time; and (2) the effects of chemical change can be adequately represented by scaling the entire vertical profile. The measured columns are divided by the corresponding theoretical columns for a subsided but chemically unchanged stratosphere, to produce dimensionless relative columns; the effect of this last operation is to remove residual effects due to variations of temperature or aircraft altitude.

The third stage is to take all measurements made within the span of a few days and sort them according to the value of PV at the point on the 440 K potential temperature (PT) surface through which the column density measurement passes. We define a set of bins in PV space, with centers spaced by 0.1×10^{-5} K m^2/kg s, and widths equal to twice this spacing. The average bin contains about 8.2 data points, but to ensure adequate sampling we require a minimum of 6 data points, achieved by widening the bin where necessary. The mean and variance are estimated for each bin. The advantage of the median is that it is a robust statistic. The advantage of the binning method is that it produces uniform sampling over a wide range of PV; the modest price paid is that the correlation length along the PV axis is variable, viz., slightly more than 2 points, on average.

The results of this 3-stage analysis are shown in Fig. 2 for HCl, O_3, HNO_3, and H_2O. Because HF is used to determine the subsidence, the corresponding HF points are all unity, by definition. The data are distributed as follows: 165 observations (per species) from flights on UT dates January 14, 16, 19, 22, and 24, 1992; 112 observations from February 17, 20, and 22; and 177 observations from March 10, 12, 14, 18, and 20. About 13 percent of the original data are not used here because observing conditions were poor, i.e., the DC-8 was flying through signal-degrading clouds, or it was changing altitude rapidly. The range of latitudes each month is nominally from 38°N (Moffett Field, California) to 90°N, except for one flight in February to 15°N (Puerto Rico). The January measurements at values of

PV $> 3.5 \times 10^{-5}$ were made at latitudes having 24 hours of darkness in January.

Discussion

The use of the (PV, PT) coordinate system to track air parcels has been discussed extensively [*e.g., Proffitt, et al.*, 1989; *Schoeberl, et al.*, 1989]. Both PV and PT are conserved along isentropic trajectories. An air parcel will experience a change in PT as a result of diabatic cooling, while a change in PV requires the gradient of the diabatic cooling rate to have a component parallel to the total vorticity vector. While the usefulness of the (PV, PT) coordinate system in analyzing in-situ data is clear, its application to remote sensing of columns requires justification.

A single measurement of column density comprises an integral along the line of sight of many air parcels, each having a different coordinate in (PV, PT) space. The column can be characterized by the value of PV at a fixed PT. The question is whether or not a column measurement made at a later time which passes through the same air parcels can be compared with the earlier measurement. The comparison would not be valid in the presence of strong wind shear, which would shuffle the air parcels. The extent of mixing could be found by trajectory analysis, but for this paper we assume that the parcels along the line of sight are co-moving.

In *Traub et al.* [1994b] it was shown that the subsidence increases dramatically between the exterior and the interior of the vortex, and that the transition occurs in the region $(1.3 - 1.7) \times 10^{-5}$ K m^2/kg s. This region is only slightly larger than the step size of the National Meteorological Center analysis from which the values of PV were derived [*Schoeberl et al.*, 1992], so that the actual transition region may be narrower.

In general, if the standard vmr_0 profiles are chosen to be representative of a typical mid-latitude region, and if the aircraft flew in unperturbed mid-latitude air outside the vortex, then the nominal relative columns outside the vortex would be unity. Inspection of Fig. 2 shows that the relative columns are clearly trending towards a value of unity as the aircraft exits the vortex. However, despite this trend, the relative columns clearly do not plateau at a value of unity well outside the vortex. There are several plausible reasons for this: (1) columns are generally latitude dependent; (2) this data set includes only one DC-8 flight well outside the vortex wall region, so the sampling is sparse; (3) the flight path may have intercepted previously perturbed air parcels; (4) PV is not a good coordinate far outside the vortex.

To compare abundances inside and outside the vortex, and taking into account the preceding discussion, we note from Fig. 2 that a region which could be reasonably assigned to the outside of the vortex is PV(outside) $= (1.3 - 1.7) \times 10^{-5}$ K m^2/kg s, and a corresponding region inside the vortex is PV(inside) $= (2.6 - 3.4) \times 10^{-5}$ K m^2/kg s. (Note that PV(outside) coincides with the subsidence transition region, which, while not truly beyond the influence of the vortex, is still well removed from the inner region.) We use these regions in the following to discuss chemical change in the vortex. Ratios are stated to the nearest 5%, and the uncertainties are conservatively estimated to be 10%.

In Fig. 2a we show the normalized HCl column density as a function of PV. The column is depleted by about (55±10)% inside the vortex relative to the vortex exterior. If we assume that the loss of HCl occurs in the coldest region of the stratosphere (PT = (360 − 560) K, or altitudes of 14–22 km inside the vortex), then a nearly total loss of HCl in this altitude range is required to account for the observed loss in column density. In-situ measurements of HCl in the Arctic vortex near 20 km observed losses of > 95% in some air parcels in January [*Webster et al.*, 1993], which were strongly correlated with increases in the ClO abundance. We observed some recovery of HCl inside the vortex in February, but overall the trends in HCl *vs.* PV changed little from January to March. The stability of the HCl gradient as a function of PV indicates that shuffling of vertical columns has little effect on our analysis.

The ozone columns plotted in Fig. 2b show trends similar to HCl. Ozone inside the vortex is depleted by roughly (35±10)% relative to the exterior. The vor-

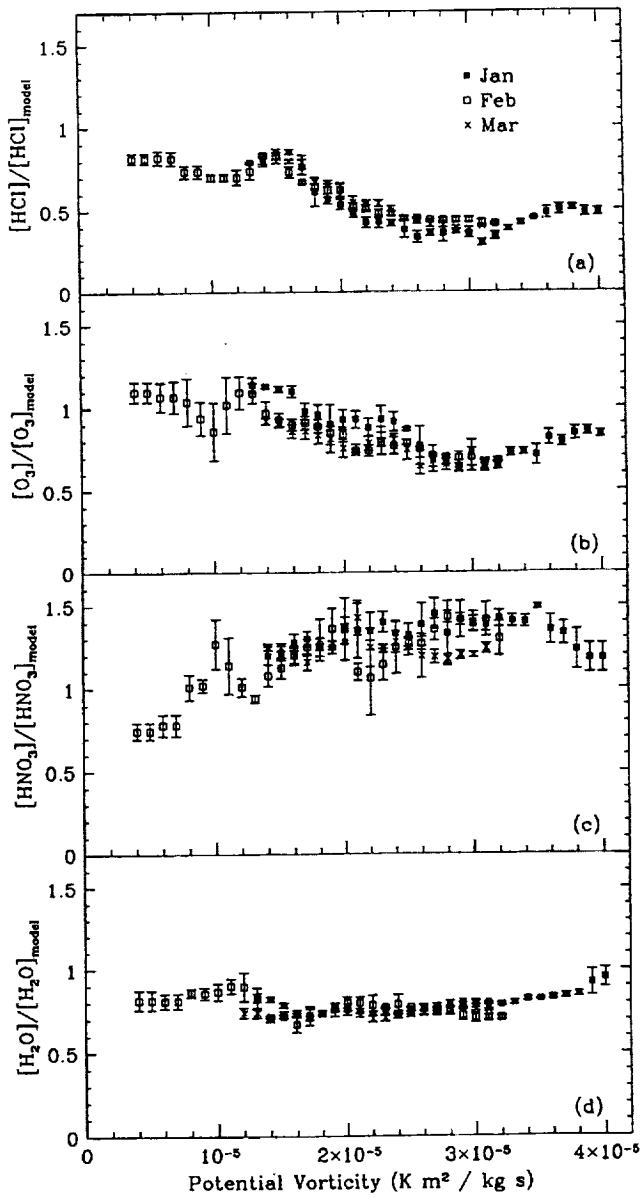

Figure 2. Monthly median values of column abundances of HCl, O_3, HNO_3, and H_2O, relative to a subsided model, during AASE II, binned by PV value.

tex interior remains relatively constant from January to March, but the depletion appears to spread to the vortex wall between January and February. The February and March measurements are quite similar. If, as for HCl, we assume that the losses are confined to the altitude range 14–22 km inside the vortex, then the ozone mixing ratio in this region must have decreased by about 70% relative to the subsided model profile. Insitu data showed losses relative to the vortex exterior in the 30–40% range in January around 17 km [*Proffitt et al.*, 1993], which is less than our estimate. However, since estimates of ozone loss depend on the choices of reference profile and altitude range, the difference between the 2 values is not surprising. The loss of ozone in the vortex wall in February may be due to dilution, by mixing with low altitude air from outside the vortex; DIAL observations of increasing aerosols in the vortex are consistent with mixing from the outside [*Browell, et al.*, 1993].

The measurements of nitric acid plotted in Fig. 2c also show signs of perturbed chemistry in the vortex, with the column density elevated by (15±10)% in the vortex wall and interior in January. Measurements in February and March indicate a gradual return to values typical of those just outside the vortex. *Toon et al.* [1992b] also observed a decrease in the HNO_3 column inside the vortex in March, and balloon measurements from Alert show unusually high HNO_3 mixing ratios inside the vortex in mid-January [*Fast et al.*, 1993], with more typical values being observed later.

The water measurements in Fig. 2d show little change, (0±10)%, across the vortex wall. This is consistent with the the absence of denitrification in Fig. 2c and also with the lack of extensive PSCs. Meteorological analysis of conditions in the Arctic vortex show that up to 30% of the 460 K surface inside the vortex was cold enough to form PSCs from late December to mid-January, but by the end of January temperatures were too warm for PSC formation [*Newman et al.*, 1993].

Conclusion

We measured column abundances above the DC-8 during AASE II, both day and night, using thermal emission spectroscopy. We removed the first-order effects of subsidence by using HF to estimate the degree of subsidence, then fitting the observed spectra with corresponding subsided profiles. We removed other secondary effects by dividing the derived column abundances by nominal mid-latitude columns. The relative columns were sorted by their corresponding PV values, and a median trend determined for each of the 3 months of observation in 1992. The resulting data demonstrate that chemical change occured inside the Artic vortex. We find that in January, in the vortex, HCl is depleted by (55±10)%, O_3 is depleted by (35±10)%, HNO_3 is enhanced by (15±10)%, and H_2O is unchanged at (0±10)%. These results show that chlorine and nitrogen were repartitioned, O_3 was chemically destroyed, and no significant sedimentation of polar stratospheric clouds occured.

Acknowledgments. This work was supported in part by NASA grant NSG 5175. We are grateful for assistance from the NASA Ames DC-8 ground and flight crews throughout the AASE II mission. We thank the referees for useful comments.

References

Anderson, J. G., and O. B. Toon, Airborne Arctic stratospheric expedition II: an overview, *Geophys. Res. Lett., 20*, 2499–2502, 1993.

Browell, E. V., C. F. Butler, M. A. Fenn, W. B. Grant, S. Ismail, M. R. Schoeberl, O. B. Toon, M. Loewenstein, and J. R. Podolske, Ozone and aerosol changes during the 1991–1992 airborne Arctic stratospheric expedition, *Science, 261*, 1155–1158, 1993.

Fast, H., C. T. McElroy, D. I. Wardle, and J. M. Rosen, Wintertime measurements of stratospheric HNO_3 as part of the ISY polar ozone project, *Geophys. Res. Lett., 20*, 2547–2550, 1993.

Johnson, D. G., K. W. Jucks, W. A. Traub, and K. V. Chance, The Smithsonian stratospheric far-infrared spectrometer and data reduction system, *submitted to J. Geophys. Res.*, 1994.

Newman, P., L. R. Lait, M. Schoeberl, E. R. Nash, K. Kelly, D. W. Fahey, R. Nagatani, D. Toohey, L. Avallone, and J. Anderson, Stratospheric meteorological conditions in the Arctic polar vortex, 1991 to 1992, *Science, 261*, 1143–1146, 1993.

Proffitt, M. H., K. K. Kelly, J. A. Powell, B. L. Gary, M.. Loewenstein, J. R. Podolske, S. E. Strahan, and K. R. Chan, Evidence for diabatic cooling and poleward transport within and around the 1987 Antarctic ozone hole, *J. Geophys. Res., 94*, 16,797–16,813, 1989.

Proffitt, M. H., K. Aikin, J. J. Margitan, M. Loewenstein, J. R. Podolske, A. Weaver, K. R. Chan, H. Fast, J. W. Elkins, Ozone loss inside the Northern polar vortex during the 1991–1992 winter, *Science, 261*, 1150–1154, 1993.

Schoeberl, M. R., L. R. Lait, P. A. Newman, R. L. Martin, M. H. Proffitt, D. L. Hartmann, M. Loewenstein, J. Podolske, S. E. Strahan, J. Anderson, K. R. Chan, and B. L. Gary, Reconstruction of the constituent distribution and trends in the Antarctic polar vortex from ER-2 flight observations, *J. Geophys. Res., 94*, 16,815–16,845, 1989.

Schoeberl, M. R., L. R. Lait, P. A. Newman, and J. E. Rosenfield, The structure of the polar vortex, *J. Geophys. Res., 97*, 7859–7882, 1992.

Toon, G. C., C. B. Farmer, P. W. Schaper, L. L. Lowes, R. H. Norton, M. R. Schoeberl, L. R. Lait, and P. A. Newman, Evidence for subsidence in the 1989 Arctic winter stratosphere from airborne infrared composition measurements, *J. Geophys. Res., 97*, 7963–7970, 1992a.

Toon, G. C., J.-F. Blavier, J. N. Solario, and J. T. Szeto, Airborne observations of the 1992 Arctic winter stratosphere by FTIR solar absorption spectroscopy, *SPIE 1715*, 457–467, 1992b.

Traub, W. A., K. W. Jucks, D. G. Johnson, M. Coffey, W. Mankin, and G. C. Toon, Comparison of column abundances from three infrared spectrometers during AASE II, *accepted by Geophys. Res. Lett.*, 1994a.

Traub, W. A., K. W. Jucks, D. G. Johnson, and K. V. Chance, Subsidence of the Arctic stratosphere as determined from thermal emission of HF, *submitted to J. Geophys. Res.*, 1994b.

Webster, C. R., R. D. May, D. W. Toohey, L. M. Avallone, J. G. Anderson, P. Newman, L. Lait, M. R. Schoeberl, J. W. Elkins, K. R. Chan, Chlorine chemistry on polar stratospheric cloud particles in the Arctic winter, *Science, 261*, 1130–1134, 1993.

K. Chance, D. Johnson, K. Jucks, and W. Traub, Smithsonian Astrophysical Observatory, 60 Garden Street, Cambridge, MA 02138; email: chance@cfa.harvard.edu, dgj@cfa.harvard.edu, jucks@cfa.harvard.edu, traub@cfa.harvard.edu

(received March 14, 1994; accepted May 18, 1994.)

APPENDIX C

Remote Sensing Measurements of HBr and HOBr and Implications for Bromine Partitioning in the Stratosphere

Remote Sensing Measurements of HBr and HOBr and Implications for Bromine Partitioning in the Stratosphere

D. G. JOHNSON, W. A. TRAUB, K. V. CHANCE, AND K. W. JUCKS

Harvard-Smithsonian Center for Astrophysics, Cambridge, Massachusetts

We determine mixing ratio profiles of HBr and HOBr in the stratosphere with precisions up to 1.3 and 4.6 parts per trillion, respectively, using the combined data from 7 flights of our far-infrared spectrometer. The measurements suggest that in the range 25–35 km the mixing ratio of HBr is less than 2.5 ppt and the mixing ratio of HOBr is less than 6.4 ppt. Our measurements are in reasonable agreement with a photochemical model which includes 0 or 2% production of HBr through the reaction of BrO with HO_2, but in strong disagreement with a model including 5 or 10% HBr production.

INTRODUCTION

Anthropogenic emission of methyl bromide and the halons has the potential to cause greater ozone losses than emissions of chlorofluorocarbons and hydrochlorofluorocarbons, in part because nearly 50% of the bromine released into the stratosphere is believed to exist in reactive forms, as compared to a few percent of the chlorine [*World Meteorological Organization (WMO)*, 1992]. Already, at a concentration of only 0.5% that of chlorine, catalytic cycles involving bromine account for 25% of the ozone loss in the Antarctic ozone hole and a few percent of the total ozone loss rate at mid-latitudes [*McElroy et al.*, 1992].

Accurate assessment of the ozone depletion potential (ODP) of brominated compounds requires an understanding of the partitioning of stratospheric bromine between reactive species (Br, BrO) and reservoir species (HBr, $BrNO_3$, and HOBr). Their low abundance has made measurement of bromine species difficult, which is unfortunate because there is still considerable uncertainty in the reaction rates used in photochemical models and comparison with observations would build confidence in model predictions.

For example, the reaction rate for $BrO + HO_2$ at 298 K was recently found to be 6 times faster than previously believed [*Poulet et al.*, 1992]. The effect of the faster reaction rate is to increase the abundance of HOBr at the expense of BrO, assuming that the only products are HOBr and O_2. Models which include some production of HBr through this reaction predict even less BrO, resulting in a smaller ODP for brominated compounds such as methyl bromide (CH_3Br) [*Poulet et al.*, 1992; *Ko et al.*, 1994]. While not observed at room temperature, the existence of an HBr channel is not ruled out at lower temperatures by the work of *Poulet et al.* [1992]. Recent observations of a lower than expected ClO/HCl ratio [*Stachnik et al.*, 1992; *Chance et al.*, 1995] could be explained by the existence of an analogous channel in the reaction of ClO with HO_2 or OH [*Tuomi and Bekki*, 1993; *McElroy and Salawitch*, 1989].

The measurements presented in this paper expand on earlier work [*Traub et al.*, 1992] in which we combined measurements from 3 balloon flights to produce an upper limit for HBr of 4 parts per trillion (ppt) at an altitude of 32 km. In the present work we combine data from 7 balloon flights to produce mixing ratio profiles of HBr and HOBr from 22–38 km.

MEASUREMENTS

The FIRS-2 spectrometer and data reduction system are described in detail elsewhere [*Johnson et al.*, 1994]. We observe the stratosphere in thermal emission from a balloon platform, recording infrared spectra continuously during both day and night. The instrument scans the Earth's limb, taking data for tangent heights ranging from the balloon altitude down to the tropopause, at which point the atmosphere becomes opaque throughout most of our wavelength range.

The launch dates and hours of data at float for the flights analyzed here are as follows: May 12, 1988, 16.6 hours; September 26, 1989, 23.1 hours; June 4, 1990, 28.1 hours (only the final 9 hours used here); May 29, 1992, 8.7 hours; September 29, 1992, 7.8 hours; March 23, 1993, 6.7 hours; and May 22, 1994, 22.0 hours. The 1988 flight was launched from Palestine, TX and the 1993 flight was launched from Daggett, CA; all other flights were launched from Ft. Sumner, NM. We bin the spectra by elevation angle, flight, and time of day to produce average limbscans for day and (or) night for each flight. Mixing ratio profiles are produced for each average limbscan.

Spectroscopic parameters for the HBr lines used in this analysis are taken from the Smithsonian Astrophysical Observatory (SAO) line database SAO92 [*Chance et al.*, 1994]. Line positions and strengths for HOBr are calculated from the constants measured by *Koga et al.* [1989]. Because the HOBr lines are very weak and unresolved in our spectra, we ignore the hyperfine splitting and use a default value of $0.06\,cm^{-1}atm^{-1}$ for the collisional broadening. Lines for both ^{79}Br and ^{81}Br are included.

We use the rotational lines near 99.9 and 116.4 cm^{-1} for HBr mixing ratio retrievals. Our average HBr sensitivity is 6 ppt for a single measurement (fitting a single line in a single averaged spectrum). The line strengths for HOBr are considerably weaker, but there are more lines in our spectra. We fit rotational lines of HOBr at 112.1, 146.3, 147.7, 149.8, 155.3, and 155.9 cm^{-1}, as well as Q branches at 140.0 and 179.4 cm^{-1}. Our average sensitivity for HOBr is about 45 ppt per measurement of a single line or Q branch. For comparison, a photochemical model starting with 20 ppt of inorganic bromine and using reaction rates and photolysis cross sections recommended by *DeMore et al.* [1992] (including the faster rate for BrO + HO_2) predicts mixing ratios for HBr and HOBr of 0.2–0.4 and 1–6 ppt, respectively [*Ko et al.*, 1994]. Therefore the signal-to-noise ratio (SNR) is roughly 0.05 for either species, and one does not expect spectral features of HBr or HOBr to be visible above the noise level in FIRS-2 spectra. However, to the extent that the sensitivity is limited by random noise, we can average many measurements together to increase the sensitivity (as discussed below). While we carefully choose the fitting windows to avoid interfering lines of other molecules, there is always the possibility that uncatalogued lines are present which could bias the average towards high values. Because of this possibility one might more conservatively consider the average mixing ratios to be upper limits, but in the discussion which follows we will treat them as unbiased measurements.

For the HBr analysis we formed 1 daytime average limbscan each for the May 1988, June 1990, May 1992, and September 1992 flights; 2 daytime averages for the September 1989 flight (one for the first day and one for the second); and 4 daytime averages for the May 1994 flight (three for the first day and 1 for the second). We also formed 1 nighttime average each for the May 1988, September 1989, and March 1993 flights; and 2 for the May 1994 flight. Because the HOBr lines are so much weaker, we formed a single daytime and a single nighttime average for the 1994 flight. Multiplying the number of average limbscans by the number of spectral windows used to fit each molecule gives 20 daytime and 10 nighttime HBr measurements per elevation angle, and 56 daytime and 32 nighttime HOBr measurements. Considering only the 5 elevation angles with the highest precision leaves a total of 150 and 440 independent measurements of HBr and HOBr, respectively.

ANALYSIS

Our fitting procedure estimates the random error in each measurement from the variance of the residuals, the number of degrees of freedom, and the correlations between the parameters being fitted. Because of the small number of degrees of freedom one expects to produce some measurements with deceptively small errors. In addition, some regions of some spectra are noisier than others and produce poor measurements. In the following we determine weighted average mixing ratio profiles using standard methods, but we exclude potentially bad measurements from the average using statistical criteria.

We consider each measurement x_i and variance ${\sigma_i}^2$ to define a subpopulation drawn from a parent population with mean x_0 and variance ${\sigma_0}^2$. The goal is to estimate (x_0, σ_0) from the set of (x_i, σ_i); the uncertainty in the estimate of x_0 is given by $\sigma_0/\sqrt{n}$, where n is the number of measurements [for example, *Anderson*, 1989]. First, we estimate (x_0, σ_0) from the full set of measurements using $x = \sum w_i x_i / \sum w_i$ and $\sigma^{-2} = \sum w_i / n$, where $w_i = 1/{\sigma_i}^2$ and (x, σ) are the estimates of (x_0, σ_0). Next, we reject outliers ($|x_i - x| > 2.5\sigma_i$), measurements with large errors ($\sigma_i > 2.5\sigma$), and measurements with small errors ($\sigma_i < \sigma/2.5$). We believe that such measurements probably do not belong to the parent population and should not be included in the weighted average. The process is repeated until no more points are rejected. A total of 28% of the measurements are rejected, usually because of large individual errors. Fewer than 3% of the measurements are rejected because of small errors. We compute the average altitudes with the same weights used to calculate the average mixing ratios.

RESULTS AND DISCUSSION

We present the final HBr and HOBr mixing ratio profiles in Tables 1 and 2. All errors are 1σ, and include random errors only. Some of the mixing ratios are negative, which is not physically meaningful, but is certainly statistically meaningful. Our nighttime measurement of HOBr at 22 km is probably too high, since it implies that all the inorganic bromine at that altitude is in the form of HOBr, but this measurement has a low SNR (about 3). The weighted average mixing ratios in the range 25–35 km are 1.9 ± 0.6 and 3.9 ± 2.5 ppt for HBr and HOBr, respectively, which can be interpreted as upper limits of 2.5 and 6.4 ppt. For comparison, the average mixing ratios calculated without rejecting any measurements are 2.0 ± 0.6 and 8.8 ± 2.2 ppt for HBr and HOBr; rejecting one measurement with suspiciously high precision changes the HOBr average to 6.3 ± 2.4 ppt.

Table 1. HBr Mixing Ratio Profiles

Day		Night	
z, km	[HBr], ppt	z, km	[HBr], ppt
38.0	7.2 ± 5.5	38.6	1.7 ± 6.3
33.0	2.5 ± 1.6	33.3	1.2 ± 1.5
29.2	3.2 ± 1.4	29.2	0.6 ± 1.7
25.6	2.3 ± 1.2	25.9	0.4 ± 2.0
21.7	-3.8 ± 1.9	22.4	4.1 ± 3.0

Combining mixing ratio profiles from many mid-latitude balloon flights is equivalent to estimating a zonal mean profile, so our measurements can be compared to the results of 2-D models. We compare our average day and night profiles for HBr and HOBr to several different model calculations in Figures 1 and 2. The model profiles are labeled A, B, C, and D. Profile A was calculated using reaction rates and photolysis cross sections taken from the 1992 Jet Propulsion Laboratory

Table 2. HOBr Mixing Ratio Profiles

Day		Night	
z, km	[HOBr], ppt	z, km	[HOBr], ppt
38.1	-27.9 ± 24.6	38.4	0.5 ± 29.6
33.2	3.8 ± 6.5	33.4	13.4 ± 7.4
29.3	1.7 ± 5.7	29.3	4.4 ± 6.5
25.8	0.3 ± 4.6	25.9	6.7 ± 7.0
22.1	8.4 ± 6.4	22.6	21.3 ± 6.1

(JPL) recommendation [*DeMore et al.*, 1992]; profile B uses the same reaction rates but includes a 2% yield of HBr from the reaction of BrO and HO_2; profile C includes a 5% yield of HBr; and profile D includes a 10% yield. Daytime and nighttime averages are shown. All model profiles were calculated using the Atmospheric and Environmental Research 2-D model (M. K. W. Ko, private communication, 1994), assuming 19 ppt of total inorganic bromine. The profiles correspond to average conditions on May 15 at at a latitude of 38 degrees north (about 4 degrees north of Ft. Sumner). Results for 28 degrees north and for September are similar.

As shown in Figure 1, the measurements of HBr are in good agreement with profiles A and B. The data are not consistent with profiles C or D, indicating that the branching ratio for HBr is less than 5% and may be 0. This agrees with the work of *Mellouki et al.* (1994), who concluded that the HBr branching ratio is less than 0.01% under atmospheric conditions by measuring the rate of the reverse reaction, O_3 + HBr. Indeed, there seems to be little evidence for a large additional source of HBr, unlike the situation for HCl [*Stachnik et al.*, 1992; *Chance et al.*, 1995]. Simultaneous measurements of BrO and HBr would provide a more direct measurement of bromine partitioning by eliminating assumptions about the total bromine concentration. From Figure 2 it is clear that profiles A–D are all consistent with the HOBr data, but there is insufficient precision in the measurements to distinguish between them. The sense of the day-night differences in the modeled HOBr disagrees with the measurements at a low level of significance. The data also seem to indicate a diurnal variation in HBr which is not reproduced by the model, but again the difference is comparable to the measurement precision.

Assuming that the errors are random, we can perform a more quantitative comparison of the models with the data by computing the χ^2 statistic. There are 20 degrees of freedom in the combined data set (5 altitudes, 2 times of day, and 2 molecules, with no free parameters). For model profile A, $\chi^2 = 32$, which indicates agreement at about the 5% confidence level (CL) (or equivalently, the model and data disagree at the 95% CL, analogous to a 2σ difference). Profile B matches the data nearly as well, with $\chi^2 = 38$. Profiles C and D, with $\chi^2 = 83$ and 176 respectively, are inconsistent with the data at a CL > 99%. If we ignore the HBr measurements at 22 km the confidence limits for profiles A and B increase to 10 and 20%, respectively, while profiles C and D are still rejected with a very high CL. However, we have no a priori reason to reject these points.

CONCLUSION

The HBr and HOBr measurements presented here are consistent with a model which assumes 19 ppt of total inorganic bromine and conventional chemistry. The data are also consistent with a model which includes 2% production of HBr through the reaction of BrO with HO_2, but are highly inconsistent with a 5 or 10% production of HBr.

Acknowledgments. We gratefully acknowledge support from NASA's Upper Atmosphere Research Program in the form of grant NSG 5175. We thank Darin Toohey for helpful comments and Malcom Ko for providing the model calculations together with useful suggestions. Technical assistance for the balloon flight was provided by the Jet Propulsion Laboratory and the National Scientific Balloon Facility.

REFERENCES

Anderson, H. L. (Ed.), *A Physicist's Desk Reference: The Second Edition of Physics Vade Mecum*, p. 21, American Institute of Physics, New York, 1989.

Chance, K. V., K. W. Jucks, D. G. Johnson, and W. A. Traub, The Smithsonian Astrophysical Observatory database SAO92, *J. Quant. Spectrosc. Radiat. Transfer, 52*, 445–457, 1994.

Chance, K. V., W. A. Traub, D. G. Johnson, K. W. Jucks, P. Ciarpallini, R. A. Stachnik, R. J. Salawitch, and H. A. Michelsen, Simultaneous measurements of stratospheric HO_x, NO_x, and Cl_x: Comparison with a photochemical model, in preparation, 1995.

DeMore, W. B., S. P. Sander, D. M. Golden, R. F. Hampson, M. J. Kurylo, C. J. Howard, A. R. Ravishankara, C. E. Kolb, and M. J. Molina, Chemical kinetics and photochemical data for use in stratospheric modeling, *JPL Publication 92-20*, 1992.

Johnson, D. G., K. W. Jucks, W. A. Traub, and K. V. Chance, Smithsonian stratospheric far-infrared spectrometer and data reduction system, *J. Geophys. Res.*, in press, 1994.

Ko, M. K. W., N.-D. Sze, J. M. Rodriguez, and D. K. Weisenstein, Ozone depletion potential of CH_3Br: Sensitivity to uncertainties in rate data, in *Proceedings of the Methyl Bromide State of the Science Workshop*, p. 19 and App. C., Science and Policy Associates, Inc., 1994.

Koga, Y., H. Takeo, S. Kondo, M. Sugie, C. Matsumura, G. A. McRae, and E. A. Cohen, The rotational spectra, molecular structure, dipole moment, and hyperfine constants of HOBr and DOBr, *J. Mol. Spectrosc., 138*, 467–481, 1989.

McElroy, M. B., R. J. Salawitch, Changing composition of the global stratosphere, *Science, 243*, 763–770, 1989.

McElroy, M. B., R. J. Salawitch, and K. Minschwaner, The changing stratosphere, *Planet. Space Sci., 40*, 373–401, 1992.

Mellouki, A., R. K. Talukdar, and C. J. Howard, Kinetics of the reactions of HBr with O_3 and HO_2: The yield of HBr from HO_2 + BrO, *J. Geophys. Res., 99*, 22949–22954, 1994.

Poulet, G., M. Pirre, F. Maguin, R. Ramaroson, and G. Le Bras, Role of the BrO + HO_2 reaction in the stratospheric chemistry of bromine, *Geophys. Res. Lett., 19*, 2305–2308, 1992.

Stachnik, R. A., J. C. Hardy, J. A. Tarsala, and J. W. Waters, Submillimeterwave heterodyne measurements of stratospheric ClO, HCl, O_3, and HO_2: First results, *Geophys. Res. Lett., 19*, 1931–1934, 1992.

Tuomi, R. and S. Bekki, The importance of the reactions between OH and ClO for stratospheric ozone, *Geophys. Res. Lett., 20*, 2447–2450, 1993.

Traub, W. A., D. G. Johnson, K. W. Jucks, and K. V. Chance, Upper limit for stratospheric HBr using far-infrared thermal emission spectroscopy, *Geophys. Res. Lett., 19*, 1651–1654, 1992.

World Meteorological Organization, Global Ozone Research and Monitoring Project, Scientific assessment of ozone depletion: 1991, pp. 4.15, 8.13, *Rep. No. 25*, Geneva, Switzerland, 1992.

Figure 1. A comparison of the average daytime (open circles) and nighttime (solid circles) HBr mixing ratio profiles with calculated profiles A (solid), B (dotted), C (short dash), and D (long dash). Daytime average model profiles are indicated by the light lines, and nighttime averages by the heavy lines. The profile calculations are described in the text.

Figure 2. A comparison of the average daytime (open circles) and nighttime (solid circles) HOBr mixing ratio profiles with calculated profiles A (solid), B (dotted), C (short dash), and D (long dash). Daytime average model profiles are indicated by the light lines, and nighttime averages by the heavy lines. The profile calculations are described in the text.

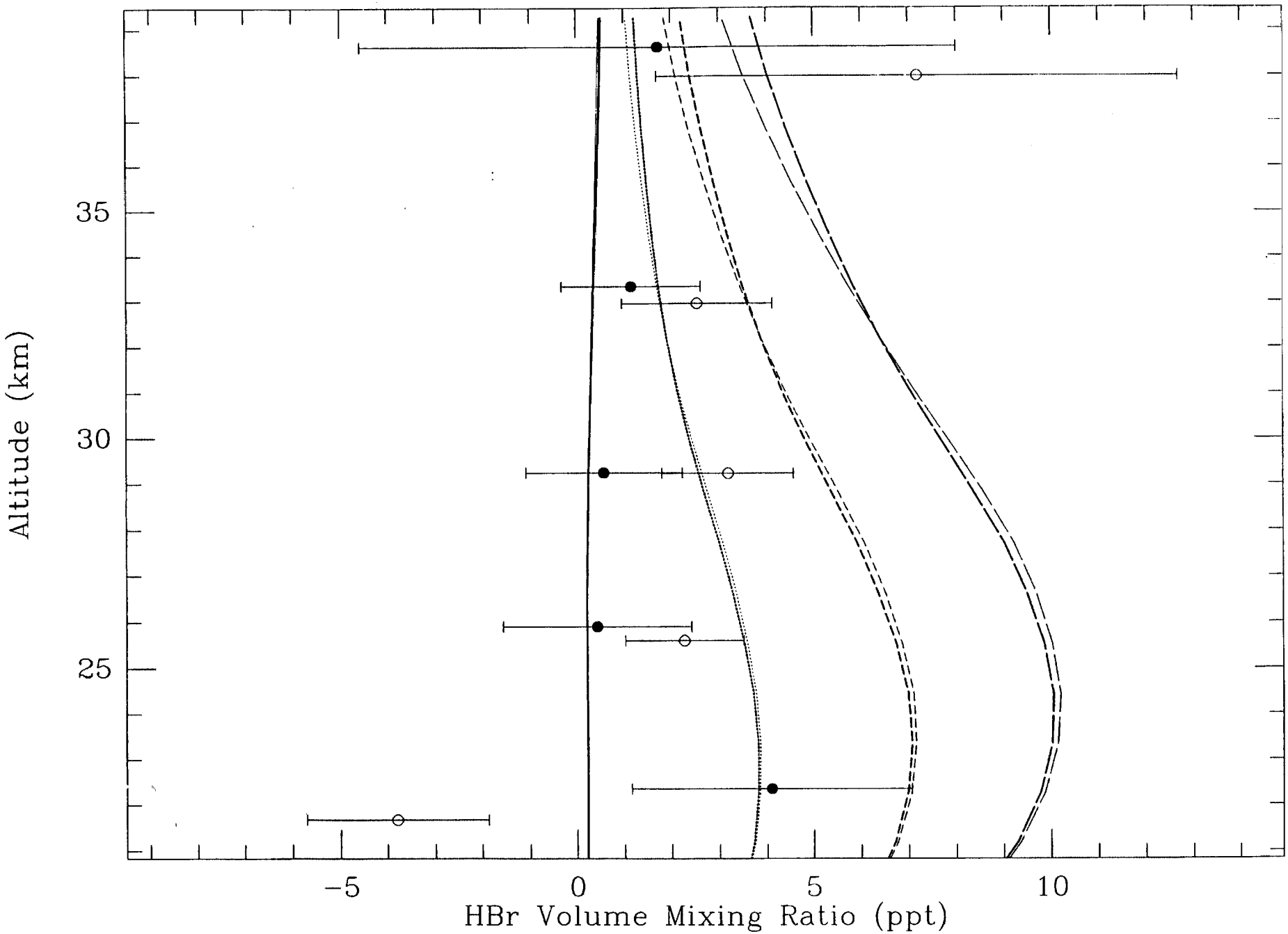
Altitude (km)
35
30
25
−5
0
5
10
HBr Volume Mixing Ratio (ppt)

APPENDIX D

Estimating the Abundance of ClO from Simultaneous Remote Sensing Measurements of HO_2, OH, and HOCl

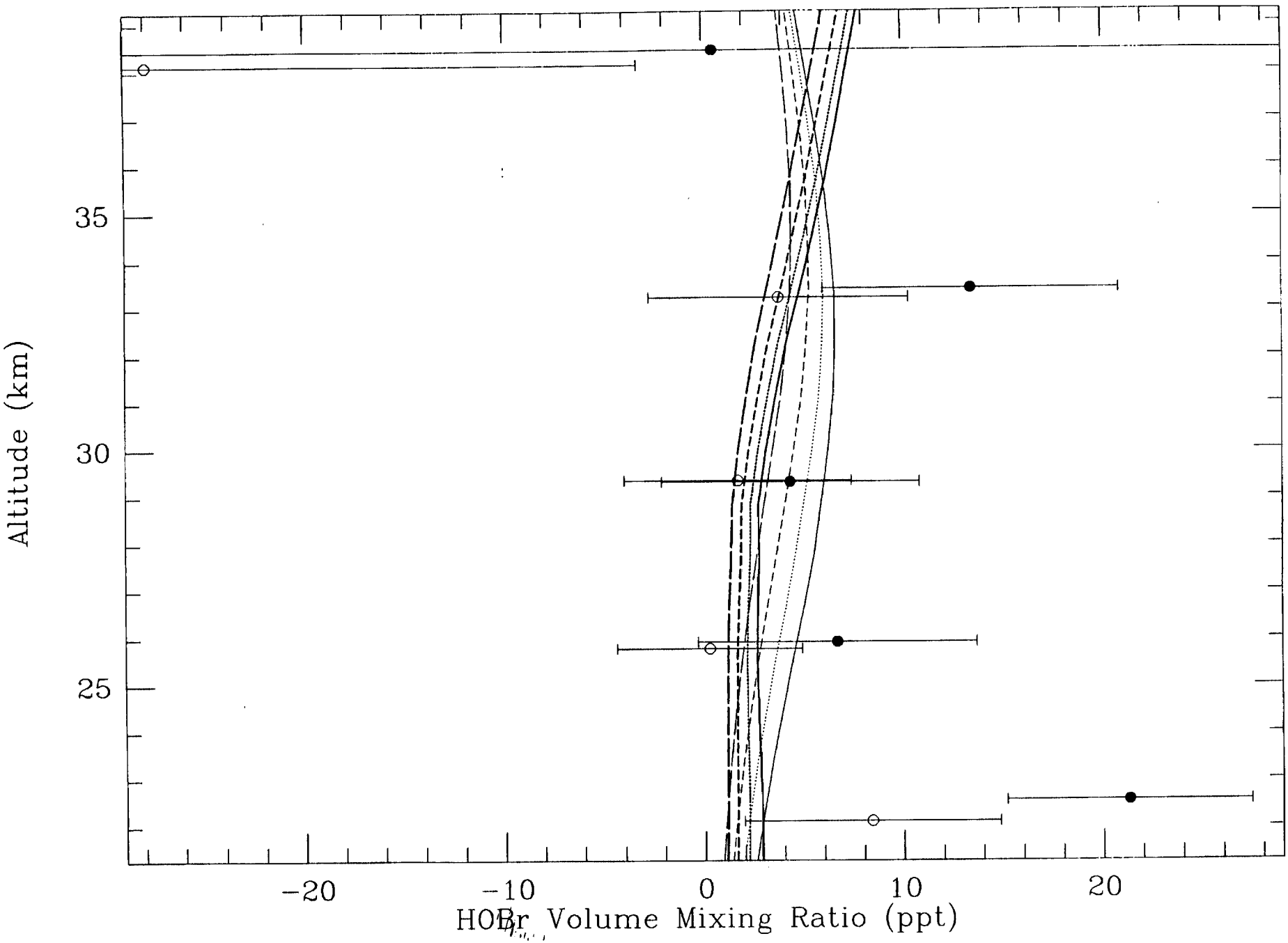
Altitude (km)
35
30
25
−20
−10
0
10
20
HOBr Volume Mixing Ratio (ppt)

Estimating the Abundance of ClO from Simultaneous Remote Sensing Measurements of HO_2, OH, and HOCl

D. G. JOHNSON, W. A. TRAUB, K. V. CHANCE, AND K. W. JUCKS

Harvard-Smithsonian Center for Astrophysics, Cambridge, Massachusetts

R. A. STACHNIK

Jet Propulsion Laboratory, Pasadena, California

Using a simple photochemical model we derive the mixing ratio profile of ClO in the altitude range 20–38 km from simultaneous measurements of HO_2, OH, HOCl, temperature, pressure, and ozone. The measurements were made with the FIRS-2 far-infrared spectrometer during a balloon flight on September 29, 1992. We compare the derived ClO with the ClO profile obtained by the SLS instrument while flying on the same gondola. The good agreement between the two profiles validates our simple model and confirms the relevant rate constants and photolysis cross sections.

INTRODUCTION

In the daytime stratosphere the relative abundance of hypochlorous acid (HOCl) and chlorine monoxide (ClO) is determined by the reactions

$$ClO + HO_2 \rightarrow HOCl + O_2 \quad (1)$$

$$HOCl + OH \rightarrow H_2O + ClO \quad (2)$$

$$HOCl + h\nu \rightarrow OH + Cl \quad (3)$$

with rate constants k_1, k_2, and j_3 respectively. Of the other gas phase reactions listed in JPL92-20 [*DeMore et al.*, 1992], the next most important source and loss reactions are slower by factors of 4000 and 6 than reactions 1 and 2, respectively.

Under some conditions, the reaction of $ClONO_2$ and H_2O on aerosol surfaces may provide another significant source of HOCl:

$$ClONO_2 + H_2O(l) \rightarrow HOCl + HNO_3 \ . \quad (4)$$

The probability of reaction 4 on sulphate aerosols decreases rapidly with increasing temperature, changing from 3×10^{-3} at 215 K to 3×10^{-4} at 295 K [*DeMore et al.*, 1992]. For aerosol surface area densities of $0.5\mu m^2/cm^3$, typical of background conditions [*World Meteorological Organization (WMO)*, 1991], reaction 4 is 10^3 to 10^4 times slower than reaction 1. At very low temperatures, in the presence of polar stratospheric clouds, or under extreme aerosol conditions, the heterogeneous reaction will have a significant effect on the HOCl abundance. However, for conditions typical of the mid-latitude stratosphere, reaction 4 can be ignored.

Recent work indicates that the rate constant for the reaction of HOCl with O-atoms at room temperature is 20 times higher than the value adopted in JPL92-20 [*Vogt and Schindler*, 1992], making it comparable in importance to the reaction with OH. However, since the reaction with atomic oxygen is believed to have a very large activation energy compared to reaction 2, this reaction will be less significant at cold stratospheric temperatures. Furthermore, since the rate of reaction 2 is already less than 1% of the photolysis rate at solar noon in the mid-latitudes, the small additional loss due to the O-atom reaction is negligible, and will not be considered in the present analysis.

By balancing the creation and destruction rates of HOCl we derive the following expression for ClO:

$$[\mathrm{ClO}] = [\mathrm{HOCl}]\frac{j_3 + k_2[\mathrm{OH}]}{k_1[\mathrm{HO_2}]} \tag{5}$$

We justify the assumption of steady-state by noting that, at a solar zenith angle of 55°, the estimated photolysis rate (see below) implies an HOCl half-life of 22–36 minutes in the middle stratosphere; this is sufficiently short that we can assume ClO and HOCl to be constant equilibrium with each other during the day.

We use Eq. 5, together with FIRS-2 measurements of HOCl, OH, HO_2, temperature, pressure, and ozone, to estimate the abundance of ClO in the lower to middle stratosphere. We calculate the rate constants k_1 and k_2 using the measured temperature profile and data from JPL92-20. We use the atmospheric radiance program LOWTRAN7 [*Kneizys et al.*, 1988] to estimate the solar flux as a function of wavelength and altitude, using our measured temperature, pressure, and ozone profiles, extended to an altitude of 100 km with the standard profiles provided with the LOWTRAN7 code. Finally, the cross section data from JPL92-20 is used to calculate j_3.

MEASUREMENTS

The mixing ratios are measured from spectra obtained with the FIRS-2 spectrometer. The instrument and data analysis methods are described in detail elsewhere [*Johnson et al.*, 1994]. The FIRS-2 is a balloon-borne infrared Fourier transform spectrometer which measures stratospheric emission spectra over the wavelength range 14–125 μm. The spectrometer views the sky through an off-axis reflecting telescope with a 0.2° field of view. The telescope elevation angle is measured with respect to a stabilized horizontal reference, with an absolute accuracy of 0.02° under calm conditions.

The data set used here is from a balloon flight launched from Ft. Sumner, New Mexico, on September 29, 1992 at 0750 MDT. The balloon reached a float altitude of 37 km at 1020 MDT, and was cut down 8 hours later. During the flight we recorded spectra at elevation angles ranging from +30° to −4.62°, corresponding to a minimum tangent altitude of 16.6 km. For this analysis we have selected a 2.6 hour subset of the data, centered at 1530 MDT, having a mean solar zenith angle of 55°.

Initial temperature and pressure profiles used in the analysis are derived from radiosonde data reported by stations near the flight track. The temperatures are corrected using FIRS-2 measurements of the 15μm band of CO_2. Once the temperature profile has been measured, the pointing angles are corrected using a different portion of the CO_2 spectrum. The rms corrections to temperature and pointing angle are 3.4 K and 0.06° elevation, respectively.

We select a number of spectral windows for each molecule to be analyzed. Each window contains one or several emission lines which are relatively isolated from the lines of other species. We use a non-linear least-squares program to fit the mixing ratio profile to the set of spectra in onion-peeling fashion. We derive independent mixing ratio profiles for each spectral window, and then average the results together to produce the final profile.

In order to evaluate Eq. 5 we need profiles for HOCl, HO_2, and OH, as well as the temperature, pressure, and ozone profiles which are used to calculate k_1, k_2, and j_3. Descriptions of our HOCl and HO_2 measurements for other balloon flights have appeared elsewhere [*Chance et al.*, 1989; *Traub et al.*, 1990], and retrievals for OH and O_3 are similar. We average together results from 24 spectral windows for the final O_3 profile, 7 windows for HOCl, 5 windows for HO_2, and 8 windows for OH.

RESULTS AND DISCUSSION

We present the measured profiles and estimated error (1σ) in Table 1. The error includes the statistical fitting error as well as systematic errors in calibration, elevation angle, and spectroscopic parameters. The statistical error dominates for all the molecules presented in the table. We also present in Table 1 the calculated photolysis half-life of HOCl and the ClO abundance estimated using Eq. 5. The ClO confidence limits include the uncertainties in HO_2, HOCl, and OH, but not the uncertainties in the reaction rate constants or photolysis cross section.

TABLE 1. Measured and calculated profiles from FIRS-2

z(km)	P(mb)	T(K)	O_3(ppm)	HO_2(ppt)	OH(ppt)	HOCl(ppt)	$t_{\frac{1}{2}}$(min)	Estimated ClO(ppt)
20.4	54.0	212	1.8 ± 0.3	14 ± 10	2.7 ± 1.1	-4 ± 13	36	-4 ± 13
24.5	28.2	219	4.8 ± 0.2	16 ± 7	2.9 ± 0.8	44 ± 9	33	86 ± 43
28.3	15.8	224	6.3 ± 0.3	26 ± 8	7.6 ± 1.0	76 ± 11	29	220 ± 70
32.4	8.55	232	8.4 ± 0.4	51 ± 13	30 ± 3	142 ± 16	26	480 ± 130
37.2	4.22	238	8.0 ± 0.5	154 ± 33	121 ± 8	109 ± 30	22	330 ± 120

In Fig. 1 we show a comparison of our estimated ClO profile with a profile obtained simultaneously by the SLS instrument [*Stachnik et al.*, 1992]. The measured and estimated profiles are in good agreement, having a χ^2 of 4.3 with 4 degrees of freedom, excluding the measurement at 20 km. The large difference at 20 km is puzzling, considering the good agreement at other altitudes.

The effect of errors in j_3 and k_1 is potentially quite large. The estimated uncertainty in the total photolysis cross section is 40%. Due to uncertainty in the temperature dependence the value of k_1 at 215 K is known only to within a factor of 2 or 3. Ignoring the uncertainty in k_2, the abundance of ClO as estimated by Eq. 5 could be off by as much as a factor of 4. The good agreement in Fig. 1 indicates that the systematic error is much smaller than this, and probably is comparable to the measurement uncertainties (25–35%).

Having verified the relationship between ClO, HOCl, and HO_2, we can use FIRS data from other balloon flights to look for trends in ClO. We have retrieved measurements of HOCl and HO_2 (as well as HCl and other species) for 6 balloon flights covering the period 1988 through 1994 and plan to compare the increase in stratospheric chlorine due to anthropogenic emissions with our ClO estimates. We also note that we have an extensive set of measurements both before and after the eruption of Mt. Pinatubo in 1991, which gives us the opportunity to investigate the effects of the eruption on chlorine partitioning.

Acknowledgements. We gratefully acknowledge support from NASA's Upper Atmosphere Research Program in the form of grant NSG 5175. Part of this research was performed at the Jet Propulsion Laboratory, California Institute of Technology, under contract with NASA. Technical assistance for the balloon flight was provided by the Jet Propulsion Laboratory and the National Scientific Balloon Facility.

REFERENCES

Chance, K. V., D. G. Johnson, and W. A. Traub, Measurement of stratospheric HOCl: concentration profiles, including diurnal variation, *J. Geophys. Res., 94*, 11,059–11,069, 1989.

DeMore, W. B., S. P. Sander, D. M. Golden, R. F. Hampson, M. J. Kurylo, C. J. Howard, A. R. Ravishankara, C. E. Kolb, and M. J. Molina, Chemical kinetics and photochemical data for use in stratospheric modeling, *JPL Publication 92-20*, 1992.

Johnson, D. G., K. W. Jucks, W. A. Traub, and K. V. Chance, The Smithsonian stratospheric far-infrared spectrometer and data reduction system, accepted by *J. Geophys. Res.*, 1994.

Kneizys, F. X., E. P. Shettle, L. W. Abreu, J. H. Chetwynd, G. P. Anderson, W. O. Gallery, J. E. A. Selby, and S. A. Clough, Users Guide to LOWTRAN 7, *AFGL-TR-88-0177*, 137pp, 1988.

Stachnik, R. A., J. C. Hardy, J. A. Tarsala, J. W. Waters, and N. R. Erikson, Submillimeter-wave heterodyne measurements of stratospheric ClO, HCl, O_3, and HO_2: First results, *Geophys. Res. Lett., 19*, 1931–1934, 1992.

Traub, W. A., D. G. Johnson, and K. V. Chance, Stratospheric hydroperoxyl measurements, *Science, 247*, 446–449, 1990.

Vogt, R. and R. N. Schindler, A determination of the rate constant for the reaction of HOCl with O-atoms at room temperature, *Geophys. Res Lett., 19*, 1935–1937, 1992.

WMO, *Scientific assessment of ozone depletion, Report 25*, Global Ozone Research and Monitoring Project, p. 3.13, 1991.

Appendix E

Simultaneous Measurements of Stratospheric HO_X, NO_X, and Cl_X: Comparison with a Photochemical Model

Fig. 1. A comparison of estimated and measured ClO mixing ratio profiles for the balloon flight of September 29, 1992. The measurements were made over a period of 2.6 hours with an average solar zenith angle of 55°. The SLS measurements of ClO are represented by the heavy dashed line, with the confidence limits indicated by the light dashed lines. ClO mixing ratios estimated with Eq. 5 are plotted as solid circles. All errors are 1σ.

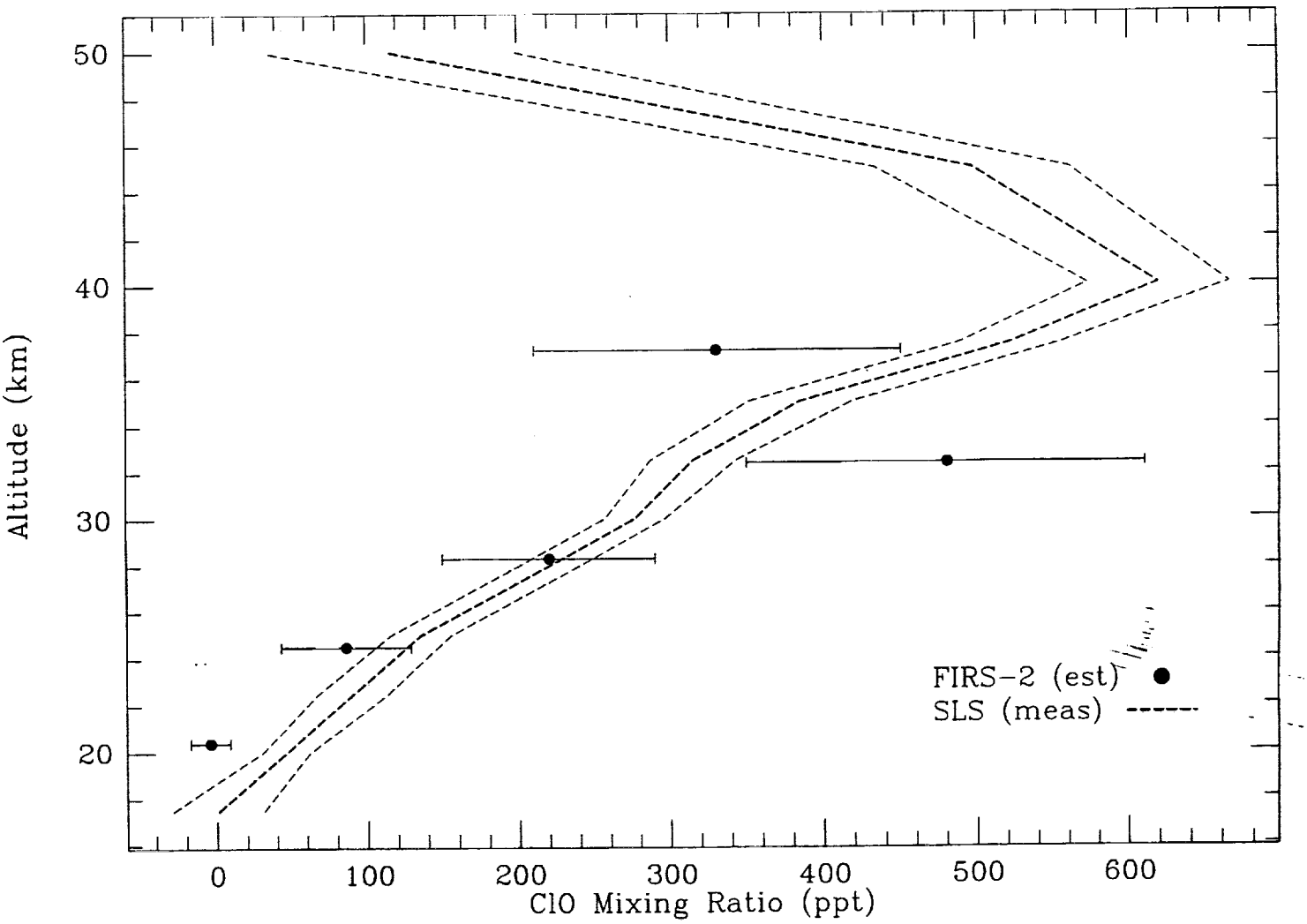

Simultaneous Measurements of Stratospheric HO_x, NO_x, and Cl_x: Comparison with a Photochemical Model

K. Chance, W.A. Traub, D.G. Johnson, K.W. Jucks, and P. Ciarpallini
Harvard-Smithsonian Center for Astrophysics, Cambridge, MA

R.A. Stachnik
Jet Propulsion Laboratory, California Institute of Technology, Pasadena, CA

R.J. Salawitch and H.A. Michelsen
Department of Earth and Planetary Sciences, Harvard University, Cambridge, MA

Received December xx, 1994; accepted January xx, 1995.

Short title: MEASUREMENTS OF STRATOSPHERIC HO_X, NO_X, AND CL_X

Abstract.

We report simultaneous measurements of the stratospheric concentration profiles of OH, HO_2, H_2O_2, H_2O, O_3, HNO_3, NO_2, N_2O, HCl, HOCl, and ClO during a midlatitude balloon flight in 1989. Measurements were made over almost an entire diurnal cycle by the Smithsonian Astrophysical Observatory Far Infrared Spectrometer (FIRS-2) and the Jet Propulsion Laboratory Balloon Microwave Limb Sounder (BMLS). We analyze these measurements using a photochemical model constrained by observations of long-lived gases. Measured HO_x species (OH and HO_2) and H_2O_2 show fair agreement with theory throughout the diurnal cycle. Measurements of HNO_3 are higher than theory near the concentration peak, while the levels of NO_2 are consistent with the model at most altitudes. Measurements of ClO and HOCl are less than predicted concentrations, suggesting a source of HCl in addition to the reaction of Cl with CH_4. Possibilities for such a source include a minor HCl + O_2 product channel for the reaction of ClO with OH, and a minor HCl and O_3 channel for the reaction of ClO with HO_2.

INTRODUCTION

Catalytic destruction of ozone from the HO_x, Cl_x, and NO_x reaction cycles is a central feature of the chemistry of the earth's ozone layer. However, it has been difficult to obtain simultaneous measurements of these radical species and their reservoirs over a range of altitudes. We report the first simultaneous measurement of HO_x, Cl_x, and NO_x species throughout the middle atmosphere. These observations represent the most comprehensive description yet obtained of the distribution of free radicals and photochemically-related gases involved in catalytic destruction of ozone.

Stratospheric balloon platforms carrying several instruments are effective at making simultaneous measurements of multiple species. The molecules currently measured by the FIRS-2 instrument include OH, HO_2, H_2O_2, H_2O, O_3, O_2, O^3P (in the mesosphere and thermosphere), HCl, HF, HOCl, HBr, CO_2, HNO_3, NO_2, N_2O, CO, HCN, and CO_2 (temperature and pressure profiles are derived from the 16 μm bands of CO_2). The BMLS instrument measures ClO and O_3. In this paper, we concentrate on measurements of HO_x (OH and HO_2), the closely-related H_2O_2, and the Cl_y and NO_y species ClO, HOCl, HCl, NO_2, and HNO_3. Measurements of radical precursors H_2O, O_3, and N_2O and temperature are used to constrain the photochemical model calculations as described below.

Measurements of the species considered in this analysis have been described in the literature. OH has been measured in the stratosphere using balloon-borne far infrared thermal emission spectroscopy [Kendall and Clark, 1980; Traub *et al.*, 1991; Carli *et al.*, 1989; Park and Carli, 1991; Pickett and Peterson, 1993], in situ resonance fluorescence [Stimpfle *et al.*, 1990; Wennberg *et al.*, 1990; Wennberg *et al.*, 1994], and balloon-borne lidar [Heaps *et al.*, 1985]. Ground-based measurements that include the stratospheric content as a part of the total column have also been made [Burnett *et al.*, 1988; Iwagami *et al.*, 1995]. The measurements presented here are the first to include the altitude profile in the stratosphere and its time variation through most of a diurnal cycle. HO_2 has been measured in remote sensing by balloon-borne far infrared thermal emission spectroscopy [Traub *et al.*, 1990; Park and Carli, 1991] and submillimeter heterodyne spectroscopy [Stachnik *et al.*, 1992], and by ground-based millimeter-wave spectroscopy [de Zafra *et al.*, 1984]. HO_2 has also been measured in situ with two techniques: chemical conversion followed by resonance fluorescence [Anderson *et al.*, 1981; Stimpfle *et al.*, 1990; Wennberg *et al.*, 1994], and matrix isolation, followed by ESR spectroscopic analysis [Helten *at al.*, 1984]. H_2O_2, which is photochemically closely related to OH and HO_2, has only been measurable in the stratosphere using far infrared thermal emission spectroscopy [Chance and Traub, 1987; Chance *et al.*, 1991; Park and Carli, 1991]. Stratospheric NO_2 has been well-determined using infrared and visible measurement techniques [Roscoe *et al.*, 1990; Russell *et al.*, 1988; Webster *et al.*, 1990]; to our knowledge, the present study is the first quantitative determination of its concentration profile using far infrared emission spectroscopy. Concentrations of H_2O, O_3, HNO_3, N_2O, and HCl have been measured by a number of investigators; reviews of most techniques for the measurement of these gases can be found in the reports of

the World Meteorological Organization [1986, 1989]. HOCl has been measured in far infrared thermal emission [Chance *et al.*, 1989] and in infrared solar absorption [Toon *et al.*, 1992]. ClO has been measured by remote sensing from balloon platforms [Stachnik *et al.*, 1992] and the Upper Atmosphere Research Satellite [Waters *et al.*, 1993] and by in situ experiments from balloons [Dessler *et al.*, 1993] and aircraft [Avallone *et al.*, 1993].

The strength of this set of measurements is the simultaneous observation of a large number of individual species, covering a large range of altitudes in the stratosphere and nearly one full diurnal cycle. The completeness of the data set provides a basis for examining our understanding of processes that regulate the partitioning of radicals using a photochemical model constrained by observations of the longer lived radical precursors.

BALLOON OBSERVATIONS

The observations discussed in this paper were made during a balloon flight from Ft. Sumner, NM (34 N, 104 W) on 26 September 1989. The balloon reached the float altitude of 36 km at 1105 Mountain Daylight Time (MDT) and began a gradual descent at 1235 MDT on 27 September. The flight was terminated at 1426 MDT. No data were recorded from 0430 to 0801 because of a telemetry problem. The spectra included in this study were taken mostly with the telescope pointing to 15±3° in geographic azimuth, corresponding to an average sampling latitude of 37.0 N, with the later afternoon scans on 26 September pointing to 188±3°, corresponding to an average sampling latitude of 31.8 N. Solar zenith angles corresponding to the measurement locations that are calculated below include these offsets in the sampling latitude from the actual location of the gondola.

The Smithsonian Astrophysical Observatory (SAO) FIRS-2 instrument was designed specifically to make thermal emission measurements of the stratosphere from a balloon platform. Its capabilities have been described previously [Traub *et al.*, 1991; Johnson *et al.*, 1994]. Briefly, it is a two-beam, high-resolution (0.004 cm^{-1} unapodized) Fourier transform spectrometer, which measures thermal emission in the far infrared (80-210 cm^{-1}) and mid infrared (350-700 cm^{-1}). Measurements are made at various angles above the earth's limb, with absolute pointing referenced to a gyroscope- and accelerometer-stabilized single-axis platform. Most observations with the FIRS-2 were made using a standard limb-scan sequence, which included blackbody calibration spectra, high-elevation spectra, and measurements at 0° elevation followed by measurements at elevation angles corresponding to 5 successive 4 km altitudes below the gondola float height. These measurements took place in a time sequence that included 6 minutes of integration time (2 complete spectra) at each angle. Thus, each complete limb-scan sequence took approximately 48 minutes. The results presented here are from both the daytime and nighttime portions of the flight.

The BMLS is a remote sensing heterodyne radiometer measuring thermal emission spectra near 205 GHz [Waters *et al.*, 1984]. The data presented here are an average of the data taken from 1100 to 1600 MDT on 26 September 1989. The BMLS was oriented

on the gondola to view in the same azimuth direction as the FIRS-2 instrument.

DATA ANALYSIS AND RESULTS

FIRS-2 spectra are analyzed to obtain concentration profiles using the nonlinear least-squares fitting procedure developed at the SAO [Johnson *et al.*, 1994] and the SAO92 spectral line database [Chance *et al.*, 1994]. Retrievals are based on multilayered, curved shell atmospheric models using distributions of pressure and temperature derived from radiosonde data obtained in the vicinity of the balloon flight. The temperature and pressure profiles are refined by fitting selected temperature- and pressure-sensitive portions of the 16 μm bands of CO_2. A comprehensive search for suitable spectral lines of each species has been carried out based upon line intensities, accuracy of spectral line parameters, and freedom from spectral interference. The selection includes 8 lines of OH which are above the FIRS-2 noise equivalent width detection limit of $\sim 10^{-5}$ cm^{-1} (hyperfine components are not counted as separate lines here, although they are fully included in the radiative transfer calculations), 5 lines of HO_2, the ${}^RQ_5$ branch of the lowest H_2O_2 rotational-torsional band, 6 lines of H_2O, 36 lines of O_3, 12 lines of NO_2, 7 lines of HCl, 5 R branch lines plus the Q_2 and Q_4 branches of HOCl, and numerous lines contained in 17 fitting windows in the ν_9 vibrational band of HNO_3 and 22 fitting windows in the ν_2 vibrational band of N_2O. As an example of the quality of spectra obtained in this balloon flight, Figure 1 shows portions of a single limb scan (6 minutes of integration time per spectrum) containing the best features of OH in the far infrared spectrum, the $F_1, 7/2 \leftarrow F_1, 5/2$ lines at 118 cm^{-1}. Spectral features are identified down to the FIRS-2 detection limit.

Most of the molecules measured here have altitude distributions that permit the onion-peeling retrieval process to proceed in a well-behaved fashion. Their mixing ratios are either nearly constant or decrease with increasing height above the balloon gondola. More importantly, the total amount of gas overhead is sufficiently small that the actual shape of the overhead distribution has a negligible effect on the retrieved concentrations from measurements taken at elevation angles corresponding to measurement heights below the gondola altitude.

The molecules whose concentrations increase with altitude above the gondola height, OH and HO_2 for the FIRS-2 measurements, present a greater challenge in the retrieval process because of the potential for the shape of the overhead distribution to affect concentrations retrieved at lower altitudes. This is particularly true because FIRS-2 does not fully resolve molecular lines, which have widths that are $\sim 3 \times 10^{-4}$ cm^{-1} at 40 km and decrease with increasing altitude. The effect of the shape of the overhead distribution on retrieved concentrations is investigated by assuming overhead distributions highly skewed with respect to standard model profiles (M. Allen, *private communication*, 1990). Overhead profile shapes affect the derived OH and HO_2 by 6% or less for the 0° measurements when the mesospheric concentrations of OH and HO_2 relative to the concentrations at gondola altitude are changed by as much as 25% from the values in the standard distributions. The effects on measurements made at

lower elevation angles are negligible. Line of sight column densities for OH and HO_2 are calculated using an initial-guess model profile for the molecule to be fitted and an altitude step size of 0.1 km. The fitting procedure then scales the initial profile using a retrieval grid matched to the viewing angles.

The FIRS-2 data in this study include a total of 24 limb-scan sequences: 9 from the first day of the flight (1105-1818 MDT), 3 from the second day (1011-1235 MDT), and 12 during the night (2028-0337 MDT). OH and HO_2 retrievals are performed for sums of 3 successive limb scans during the daytime for use in comparison with photochemical modeling predictions. The limitation to sums of 3 limb scan sequences is caused by the low signal to noise ratios of the measured HO_2 lines; OH can be determined well from individual limb scan sequences. All other molecules are analyzed by making separate averages of (1) all 9 limb scan sequences from 26 September, (2) all 12 limb scan sequences from the nighttime, and (3) the first 3 limb scan sequences from 27 September (the same sum of limb scans co-added for OH and HO_2 retrieval on the morning of 27 September). We do not see evidence for diurnal variation of H_2O_2, H_2O, O_3, HNO_3, N_2O, and HCl, which have long photochemical lifetimes. The sensitivity is sufficient to distinguish between the average daytime and nighttime concentrations for NO_2 and HOCl, but not to determine their diurnal variation on a finer time scale.

ClO was measured by the BMLS instrument, which uses the manifold of lines centered at 204.325 GHz for atmospheric retrievals. The data are reduced using both constrained least squares and sequential estimation fitting procedures [Waters *et al.*, 1984; Waters *et al.*, 1988]. The radiative transfer calculation is also based on multilayered curved shell models of the atmosphere, with stratospheric temperature profiles derived from local radiosonde data. The 206.132 GHz O_3 line is used to calibrate instrument pointing. The estimated uncertainty for ClO includes random spectral noise, radiometric calibration errors and spectral line parameter errors. The data presented here are an average of the ClO concentrations retrieved from 1100 MDT to 1600 MDT on 26 September 1989. During this time, little diurnal variation was seen or expected since ClO varies rapidly at sunrise and sunset, but is relatively constant during mid-day.

Results are presented for each species for the range of tangent heights that provide meaningful retrievals for the particular period of averaging. The results of the fitting and error analysis are presented in Tables 1, 2, and 3. Table 1 contains results from the first day average, the nighttime average, and the second day average. The sums for the second day include only observations made before the balloon began descending. Table 2 contains the OH and HO_2 retrievals for the four sets of short sums (3 limbs scans in each sum), 3 for the first day of the flight and 1 for the second day, which constitute the primary time-dependent measurements of HO_x from the present flight. The total FIRS-2 uncertainty estimate includes effects due to the following: nonlinear least-squares fitting of the spectra, intensity calibration of the spectra, pointing errors, overhead abundance (discussed above), determination of ambient pressure, propagation of abundance uncertainties to lower layers in the onion-peeling process, and uncertainties in the molecular parameters (including their temperature uncertainties). Further laboratory measurements may improve the spectral line parameters enough to significantly decrease

the systematic uncertainties for some molecules. The effect of diurnal variation of OH and HO_2 on the onion-peeling retrieval process (*i.e.*, concentrations in upper layers change during the limb-scanning process before observations at lower layers are completed) is found to be negligible for the present observations. Table 3 contains the BMLS measurements of ClO with 1σ errors that include all known systematic errors. Tables 1, 2, and 3 also include the measurement altitudes and average solar zenith angles for the locations of limb-sampling regions.

PHOTOCHEMICAL MODEL

The observations are compared with the calculations made with a photochemical model constrained by measured concentrations of radical precursors [Logan *et al.*, 1978; McElroy and Salawitch, 1989; Salawitch *et al.*, 1994a]. Input to the model includes vertical profiles for O_3, NO_y (defined as the sum of [NO] + [NO_2] + [HNO_3] + [$ClNO_3$] + 2[N_2O_5] + [HNO_2] + [HNO_4]), Cl_y (defined as [Cl] + [ClO] + [HCl] + [$ClNO_3$] + [HOCl] + 2[Cl_2]), H_2O, CH_4, temperature, and aerosol surface area. We have obtained input profiles for O_3, H_2O, and temperature from an average of measurements for the first day, second day, and night, interpolated to a common altitude grid. The input profile for CH_4 is derived from FIRS-2 measurements of N_2O, using a relation developed from 1985 Atmospheric Trace MOlecule Spectroscopy (ATMOS) measurements [Gunson *et al.*, 1990], adjusted for the change in concentration of CH_4 between 1985 and 1989. NO_y is derived from the FIRS-2 measurements of N_2O using correlations measured by the ER-2 aircraft and ATMOS [Loewenstein *et al.*, 1993; Russell *et al*, 1988]. Total Cl_y is estimated from its relationship with N_2O based on measurements of chlorinated organic source gases [Woodbridge *et al.*, 1994] and is adjusted to match the chlorine levels in 1989. The input profile of aerosol surface area peaks at 2×10^{-8} cm^{-1} at 16 km and is representative of non-volcanic, background conditions based on measurements by the Stratospheric Aerosol and Gas Experiment II (G.K. Yue, *private communication*, 1994). Thus, to the extent feasible, the model reflects the state of the atmosphere at the time of the balloon flight, as determined from measurements of the long-lived species that are precursors to radicals and reservoir species. Using this set of input parameters, the model is used to calculate diurnally varying concentration profiles by balancing production and loss of each species over a 24 hour period [Logan *et al.*, 1978] using reaction rates and photolysis cross sections from the current JPL recommendation [DeMore *et al.*, 1992] (JPL92). A reaction probability of 0.1 is used for the heterogeneous hydrolysis of N_2O_5 (JPL92); the formulation of Hanson *et al.* [1994] is adopted for the rate of the heterogeneous hydrolysis of $ClNO_3$. A radiative transfer model that includes Rayleigh and aerosol scattering is used to calculate photolysis rates [Prather, 1981]. The calculated rate for photolytic production of O^1D from O_3 is based on a study that allows for production of O^1D via excited ro-vibrational states of O_3 [Michelsen *et al.*, 1994]. This rate leads to ~40% enhancements in O^1D production and ~15% enhancements in concentrations of OH in the lower stratosphere relative to models using the rate given by JPL92. Additionally, the temperature dependances for the absorption cross sections

of HNO_3 are adjusted to agree with recently measured values [Burkholder *et al.*, 1993].

DISCUSSION

HO_x SPECIES

Our midday measurements of OH fall within the range of the previous measurements shown in Figure 4 of Pickett and Peterson [1993]. The variations between our measurement and previous measurements are reasonable considering the accumulated errors and atmospheric variability with latitude and season. Present measurements of HO_2 in the stratosphere are in good agreement with previous measurements summarized by Park and Carli [1991]. The strengths of the present set of observations are the simultaneous measurement of the full HO_x chemical family during a full diurnal cycle, and the ability to compare these observations with a model constrained by simultaneous measurements of H_2O and O_3, which regulate concentrations of HO_x. Similar measurements have been made in the lower stratosphere from the NASA ER-2 during the Stratospheric Photochemistry, Aerosols and Dynamics Expedition (SPADE) mission [Wennberg *et al.*, 1994; Salawitch *et al.*, 1994a; Salawitch *et al.*, 1994b]. The present work extends this type of comparison to an altitude range that includes most of the stratosphere.

Comparisons of concentrations of OH and HO_2 measured at 4 solar zenith angles (SZA) and model calculations are shown in Figure 2. Measurements are interpolated vertically to provide values on the same altitude grid as the model calculations (38, 32, 28, and 24 km) and to remove the effects of different tangent altitudes in the various sums of limb-scan sequences. The average SZAs for the measurements, which determine the average local solar time used in Figure 2, are calculated from the latitude, longitude, and viewing direction of the instrument. Measurements of OH are significantly higher (~33%) than model values at 38 km (there is a greater than 99% probability of the measured OH being higher, based upon the χ^2 for the comparison). For OH at 32 km and HO_2 at 28 km, the χ^2 values indicate about 99% probability of the observed concentrations being higher than the model values. The measurement of HO_2 at 16 hours and 28 km may be an outlier: elimination of this point reduces the χ^2 from 15, with 4 degrees of freedom, to 1.8, with 3 degrees of freedom. Except for this point, the diurnal trends for the theory and observation of OH and HO_2 are consistent. The difference between measured and modeled OH at 38 km is unlikely to be due to uncertainty in the UV flux and O_3 concentration involved in estimating the production of OH from the reaction of O^1D with H_2O since the model is constrained by the observed concentrations of O_3 (1σ uncertainties of 6-7% at this altitude) and the overhead column abundance of O_3 used in the model agrees with the column inferred from the measurements to within 10%.

Figure 3a compares the retrieved and calculated profiles of H_2O_2. With the exception of a few low measurement points in the middle of the measurement range, near 25 km, and one outlying point at 30 km (the only measurement point that disagrees with the model at the 2σ level), the measured concentrations agree reasonably well with modeled

values. The statistical comparison shows a χ^2 of 40, with 14 degrees of freedom if all points are included, indicating a high probability of disagreement over the profile shape. If the 4 points mentioned above are eliminated, the χ^2 is 9.3 for 10 degrees of freedom, corresponding to a 50% statistical probability of agreement. Consideration of only data above 30 km increases the statistical confidence level of agreement even further, suggesting that our current knowledge of the relative creation ($HO_2 + HO_2 \rightarrow H_2O_2 + O_2$) and photolysis rates for H_2O_2 is adequate.

NO_y SPECIES

Measurements of HNO_3 by FIRS-2 for this flight show very good agreement with previous balloon-borne remote and in situ measurements. Our measurements are consistent with observations of HNO_3 by BLISS at 31 km in 1988 to within the error bars [May and Webster, 1989] and are also consistent with many previous measurements at similar latitudes summarized in Figure 3 of May and Webster [1989]. However, our observation of HNO_3 are consistently 30-40% higher than retrievals by ATMOS for the northern hemisphere [Russell *et al.*, 1988], especially for altitudes below 28 km. The most likely explanation for these differences is that the measurements were taken 4 years apart, in different seasons, and at slightly different latitudes. The ATMOS measurements were obtained at slightly lower latitudes (~28°) than our measurements (32-37° N), which could explain some of the discrepancy. The fact that different vibrational bands are used by FIRS-2 and ATMOS retrievals is unlikely to cause the discrepancy, since all previous balloon measurements, including BLISS, use the same vibrational bands for retrieval as ATMOS, and the uncertainties in band strengths are about 10% [Goldman *et al.*, 1975; Giver *et al.* 1984; May *et al.*, 1987].

Figure 3b compares measured and modeled profiles for HNO_3. The measurements are about 10-30% higher at the peak of the profile (24 km) and slightly lower at the upper altitudes. Some of this discrepancy could be due to uncertainty in the spectroscopic transition intensity (~10%), which is included in the error analysis. Also, measurement uncertainties for O_3 and N_2O, used as inputs to the model, affect calculated HNO_3 at the 10% level. (N_2O is used to infer NO_y, which will have a direct effect on HNO_3.) Alternatively, errors in the NO_y/N_2O relationship could affect modeled HNO_3 in a similar manner. The total NO_y is inferred by using a correlation derived from ER-2 in situ data, which may not hold at the higher measurement altitudes in this study.

The FIRS-2 daytime observations of NO_2, shown in Figure 3c, differ slightly from previous observations [Webster *et al.*, 1990; Russell *et al.*, 1988] and from model profiles. Our measurements in the 37-40 km region are consistently $\sim 1\sigma$ higher than the previously reported measurements and model values. The nighttime measurements agree well with the model. The ability of FIRS-2 to measure NO_2 was limited at the time of this balloon flight, making it difficult to draw more definite conclusions from the comparison. Improved measurements of NO_2, enabled by improved noise performance in the far infrared channel, will become available from more recent FIRS-2 flights. This will permit more detailed evaluation of NO_y partitioning.

Cl_y SPECIES

Recently reported measurements of HCl and ClO from the Submillimeter Limb Sounder (SLS) [Stachnik *et al.*, 1992] showed that the ClO/HCl ratio was much lower than suggested by photochemical models. One proposal that would explain this is that ClO and OH react to produce HCl, as suggested by McElroy and Salawitch [1989]. JPL92 suggests a lower limit of 0% for the HCl branching ratio, with an upper limit of 14%, since production of HCl is a four-center reaction involving the breaking and making of multiple chemical bonds. Current investigations of ATMOS measurements of HCl and $ClNO_3$ are consistent with a non-zero yield of HCl from this reaction (H.A. Michelsen, unpublished results). Similarly, the possibility of production of HCl from the reaction of ClO + HO_2 may also be important for resolving the discrepancy (the JPL92 recommended branching ratio is 0% with an upper limit of 3%).

The set of measurements from this balloon flight is ideally suited for addressing partitioning within the Cl_y family. Besides the direct measurement of ClO, HCl, and HOCl, we also measure concentrations of most of the reactants (OH, HO_2, and NO_2) involved in the creation and destruction of the main reservoir species in the Cl_y family. The only important species not measured is CH_4, whose reaction with Cl is the main source of HCl. CH_4 can be estimated quite accurately from its observed correlations with N_2O [Gunson *et al.*, 1990]; (M.R. Gunson, *private communication*, 1994). The main sink for HCl is its reaction with OH to produce Cl + H_2O. As stated earlier, the modeled OH agrees well with the measured OH except at the highest measurement altitudes, suggesting that the loss rate of HCl should be well described by the model assuming the validity of the current rate constant for OH + HCl. Uncertainties in OH do not provide an explanation for discrepancies in Cl_y in the present data set.

Figure 4 shows our measurements of three Cl_y species along with model calculations, corresponding to the average SZA of the measurements, assuming different branching ratios for the production of HCl from the reaction of ClO with both OH and HO_2. The left side of the figure shows results from models incorporating a 0% branching ratio for the ClO + HO_2 reaction, and the right side shows results for a 3% branching ratio. Each panel shows three model calculations, assuming branching ratios for the ClO + OH reaction of 0%, 5%, and 10%. Assuming the total Cl_y used in the model is correct, these plots suggest that there must be some production of HCl at the expense of ClO and HOCl, possibly through one or both of these mechanisms.

In order to quantify the amount of any additional HCl production (and loss of ClO and HOCl) and to remove the uncertainty associated with model estimates of total Cl_y, we have plotted the ratios of [ClO]/[HCl] and [HOCl]/[HCl] (day and night) in Figure 5 using the same set of model branching ratios as in Figure 4. A statistical comparison of the measured ratios above 20 km and the model calculations shows improvement in the agreement with enhanced HCl production from both mechanisms, up to limits for the production of HCl given by the JPL92 recommendation. Best agreement ($\chi^2 = 23$ for 16 degrees of freedom, corresponding to a 10% confidence limit) is obtained for 10% production of HCl from ClO + OH and 3% production of HCl from ClO + HO_2. These

results are consistent with the conclusions from the recent SLS results [Stachnik *et al.*, 1992; Toumi and Bekki, 1993] as well as the ongoing analysis of ATMOS data (H.A. Michelsen, unpublished results). The sensitivity of the measurements is not sufficient to make firm conclusions about the extent of HCl production from the reaction with HO_2 relative to the reaction with OH. However, our observations indicate that production of HCl occurs by some process other than the reaction of Cl with CH_4.

CONCLUSIONS

We now have the most extensive set of measurements obtained to date of stratospheric radical species from the HO_x, Cl_x and NO_x families, and a number photochemically related gases. An atmospheric model constrained by measurements of long-lived radical precursors enables us to critically examine processes that regulate the abundance of radicals.

We have found HO_x concentrations that are largely in agreement with the model values, except for OH at the highest measurement altitudes, near 38 km. Concentrations of H_2O_2 are consistent with calculated values for 30 km and above.

Daytime concentrations of NO_2 are somewhat higher than model values at the highest measurement altitudes, and nighttime concentrations are in good agreement. Concentrations of HNO_3 are higher than model values near 25 km and slightly lower at altitudes above 32 km. The partitioning of NO_y agrees with the model to within the limited measurement capability for NO_2 at the time of this flight.

The major discrepancy between the measurements and standard model calculations is for the chlorine species HCl, ClO, and HOCl. We find enhanced concentrations of HCl and depleted levels of ClO and HOCl compared with the model. The discrepancy could be explained by small branching ratios to form HCl in the reactions of ClO with OH and/or HO_2. Uncertainty in the main HCl loss term, reaction with OH, implied by uncertainty in the OH concentration, can be ruled out as the cause of this discrepancy.

The measurement set includes most of the radical species involved in the rate-determining steps for catalytic ozone loss [Wennberg *et al.*, 1994]. Detailed comparisons are currently in progress of the contributions of the different radical families over the wide range of altitudes sampled by the FIRS-2 and BMLS instruments to photochemical loss of ozone and concurrent ozone production.

Acknowledgments. We are grateful to the Jet Propulsion Laboratory Atmospheric Ballooning Group for furnishing and supporting the gondola and to the National Scientific Balloon Facility for the balloon launch services. The work was supported by NASA Grants NSG-5175 (SAO) and NAGW-1230 (Harvard University). H.A. Michelsen was supported by an NSF Postdoctoral Research Fellowship. Part of this research was performed at the Jet Propulsion Laboratory, California Institute of Technology, under contract with NASA.

References

Anderson, J.G., H.J. Grassl, R.E. Shetter, and J.J. Margitan, HO_2 in the stratosphere: Three in situ observations, *Geophys. Res. Lett. 8,* 289–292 (1981).

Avallone, L.M., D.W. Toohey, M.H. Proffitt, J.J. Margitan, K.R. Chan, and J.G. Anderson, In situ measurements of ClO at mid-latitudes: Is there an effect from Mt. Pinatubo? *Geophys. Res. Lett. 20,* 2519–2522 (1993).

Burkholder, J.B., R.K. Talukdar, A.R. Ravishankara, and S. Solomon, Temperature dependence of the HNO_3 UV absorption cross sections, *J. Geophys. Res. 98,* 22,937–22,948 (1993).

Burnett, C.R., K.R. Minschwaner, and E.B. Burnett, Vertical column abundance measurements of atmospheric hydroxyl from 26°, 40°, 65° N, *J. Geophys. Res. 93,* 5341–5253 (1988).

Carli, B., B.M. Dinelli, F. Mencaraglia, and J.H. Park, The mixing ratio of the stratospheric hydroxyl radical from far infrared emission measurements, *J. Geophys. Res. 94,* 11,049–11,058 (1989).

Chance, K.V., and W.A. Traub, Evidence for stratospheric hydrogen peroxide, *J. Geophys. Res. 92,* 3061–3066 (1987).

Chance, K.V., D.G. Johnson, and W.A. Traub, Measurement of stratospheric HOCl: Concentration profiles, including diurnal variation, *J. Geophys. Res. 94,* 11,059–11,069 (1989).

Chance, K.V., D.G. Johnson, W.A. Traub, and K.W. Jucks, Measurement of the stratospheric hydrogen peroxide concentration profile using far-infrared thermal emission spectroscopy, *Geophys. Res. Lett. 18,* 1003–1006 (1991).

Chance, K., K.W. Jucks, D.G. Johnson, and W.A. Traub, The Smithsonian Astrophysical Observatory database SAO92, *J. Quant. Spectrosc. Radiat. Transfer 52,* 447–457 (1994).

DeMore, W.B., S.P. Sander, D.M. Golden, R.F. Hampson, M.J. Kurylo, C.J. Howard, A.R. Ravishankara, C.E. Kolb, and M.J. Molina, Chemical kinetics and photochemical data for use in stratospheric modeling, evaluation number 10, *JPL Publication 92-20,* Jet Propulsion Laboratory, Pasadena, CA (1992).

Dessler, A.E., R.M. Stimpfle, B.C. Daube, R.J. Salawitch, E.M. Weinstock, D.M. Judah, J.D. Burley, J.W. Munger, S.C. Wofsy, J.G. Anderson, M.P. McCormick, and W.P. Chu, Balloon-borne measurements of ClO, NO, and O_3 in a volcanic cloud: An analysis of heterogeneous chemistry between 20 and 30 km, *Geophys. Res. Lett. 20,* 2527–2530 (1993).

de Zafra, R.L., A. Parrish, P.M. Solomon, and J.W. Barrett, A measurement of stratospheric HO_2 by ground-based millimeter-wave spectroscopy, *J. Geophys. Res. 89,* 1321–1326 (1984).

Giver, L.P., F.P.J. Valero, D. Goorvitch, and F.S. Bonomo, Nitric-acid band intensities and band-model parameters from 610 to 1760 cm^{-1}, *J. Opt. Soc. Am. B 1,* 715–722 (1984).

Goldman, A., F.S. Bonomo, W.J. Williams, and D.G. Murcray, Statistical-band-model analysis and integrated intensity for the 21.8 μm bands of HNO_3 vapor, *J. Opt. Soc. Am. 65,* 10–12 (1975).

Gunson M.R., C.B. Farmer, R.H. Norton, R. Zander, C.P. Rinsland, J.H. Shaw, and B.-C. Gao, Measurements of CH_4, N_2O, CO, H_2O and O_3 in the middle atmosphere by the Atmospheric Trace Molecule Spectroscopy experiment on Spacelab 3, *J. Geophys. Res. 95,* 13867–13882 (1990).

Hanson, D.R., A.R. Ravishankara, and S. Solomon, Heterogeneous reactions in sulfuric acid

aerosols: A framework for model calculation, *J. Geophys. Res. 99*, 3615–3630 (1994).

Heaps, W.S., and T.J. McGee, Progress in stratospheric hydroxyl measurements by balloon-borne lidar, *J. Geophys. Res. 90*, 7913–7921 (1985).

Helten, M., W. Pätz, M. Trainer, H. Fark, E. Klein, and D.H. Ehhalt, Measurements of stratospheric HO_2 and NO_2 by matrix isolation and ESR spectroscopy, *J. Atmos. Chem. 2*, 191–202 (1984).

Iwagami, N., S. Inomata, I. Murata, and T. Ogawa, Doppler detection of hydroxyl column abundance in the middle atmosphere, *J. Atmos. Chem.*, in press (1995).

Johnson, D.G., K.W. Jucks, W.A. Traub, and K.V. Chance, The Smithsonian stratospheric far-infrared spectrometer and data reduction system, *J. Geophys. Res.*, in press (1994).

Kendall, D.J.W., and T.A. Clark, Stratospheric observation of far IR pure rotational lines of hydroxyl, *Nature 283*, 57–58 (1980).

Loewenstein M., J.R. Podolske, D.W. Fahey, E.L. Woodbridge, P. Tin, A. Weaver, P.A. Newman, S.E. Strahan, S.R. Kawa, M.R. Schoeberl, and L.R. Lait, New observations of the NO_y/N_2O correlation in the lower stratosphere, *Geophys. Res. Lett. 20*, 2531–2534 (1993).

Logan, J.A., M.J. Prather, S.C. Wofsy, and M.B. McElroy, Atmospheric chemistry: Response to human influence, *Phil. Trans. Roy. Soc. A290,* 187–234 (1978).

May, R.D., C.R. Webster and, L.T. Molina, Tunable diode laser measurements of absolute linestrengths in the HNO_3 ν_2 band near 5.8 μm, *J. Quant. Spectros. Radiat. Transfer 38*, 381–388 (1987).

May, R.D. and C.R. Webster, In situ stratospheric measurements of HNO_3 and HCl near 30 km using the Balloon-borne Laser In Situ Sensor tunable diode laser spectrometer, *J. Geophys. Res. 94*, 16343–16350 (1989).

McElroy, M.B., and R.J. Salawitch, Changing composition of the global stratosphere, *Science 243,* 763–770 (1989).

Michelsen, H.A., R.J. Salawitch, P.O. Wennberg, and J.G. Anderson, Production of $O(^1D)$ from photolysis of O_3, *Geophys. Res. Lett. 21*, 2227–2230 (1994).

Park, J.H., and B. Carli, Spectroscopic measurement of HO_2, H_2O_2, and OH in the stratosphere, *J. Geophys. Res. 96*, 22,535–22,541 (1991).

Pickett, H.M., and D.B. Peterson, Stratospheric OH measurements with a far-infrared limb observing spectrometer, *J. Geophys. Res. 98*, 20,507–20,515 (1993).

Prather, M.J., Ozone in the upper stratosphere and mesosphere, *J. Geophys. Res. 86*, 5325–5338 (1981).

Roscoe, H.K., B.J. Kerridge, S. Pollitt, N. Louisnard, J.M. Flaud, C. Camy-Peyret, C. Alamichel, J.P. Pommereau, T. Ogawa, N. Iwagami, M.T. Coffey, W. Mankin, W.F.J. Evans, C.T. McElroy, and J. Kerr, Intercomparison of remote measurements of stratospheric NO and NO_2, *J. Atmos. Chem. 10,* 111–144 (1990).

Russell III, J.M., C.B. Farmer, C.P. Rinsland, R. Zander, L. Froidevaux, G.C. Toon, B. Gao, J. Shaw, and M. Gunson, Measurements of odd nitrogen compounds in the stratosphere by the ATMOS experiment on Spacelab 3, *J. Geophys. Res. 93*, 1718–1736 (1988).

Salawitch, R. J., S. C. Wofsy, P. O. Wennberg, R. C. Cohen, J. G. Anderson, D. W. Fahey, R. S. Gao, E. R. Keim, E. L. Woodbridge, R. M. Stimpfle, J. P. Koplow, D. W. Kohn, C. R. Webster, R. D. May, L. Pfister, E. W. Gottlieb, H. A. Michelsen, G. K. Yue, J. C. Wilson, C. A. Brock, H. H. Jonsson, J. E. Dye, D. Baumgardner, M. H. Proffitt,

M. Loewenstein, J. R. Podolske, J. W. Elkins, G. S. Dutton, E. J. Hintsa, A. E. Dessler, E. M. Weinstock, K. K. Kelly, K. A. Boering, B. C. Daube, K. R. Chan, and S. W. Bowen, The distribution of hydrogen, nitrogen and chlorine radicals in the lower stratosphere: Implications for changes in O_3 due to emission of NO_y from supersonic aircraft, *Geophys. Res. Lett. 21,* 2547–2550 (1994a).

Salawitch, R. J., S. C. Wofsy, P. O. Wennberg, R. C. Cohen, J. G. Anderson, D. W. Fahey, R. S. Gao, E. R. Keim, E. L. Woodbridge, R. M. Stimpfle, J. P. Koplow, D. W. Kohn, C. R. Webster, R. D. May, L. Pfister, E. W. Gottlieb, H. A. Michelsen, G. K. Yue, M. J. Prather, J. C. Wilson, C. A. Brock, H. H. Jonsson, J. E. Dye, D. Baumgardner, M. H. Proffitt, M. Loewenstein, J. R. Podolske, J. W. Elkins, G. S. Dutton, E. J. Hintsa, A. E. Dessler, E. M. Weinstock, K. K. Kelly, K. A. Boering, B. C. Daube, K. R. Chan, and S. W. Bowen, The diurnal variation of hydrogen, nitrogen and chlorine radicals: Implications for the heterogeneous production of HNO_2, *Geophys. Res. Lett. 21,* 2554–2550 (1994b).

Stachnik, R.A., J.C. Hardy, J.A. Tarsala, and J.W. Waters, Submillimeterwave heterodyne measurements of stratospheric ClO, HCl, O_3, and HO_2: First results, *Geophys. Res. Lett. 19,* 1931–1934 (1992).

Stimpfle, R.M., P.O. Wennberg, L.B. Lapson, and J.G. Anderson, Simultaneous, in situ measurements of OH and HO_2 in the stratosphere, *Geophys. Res. Lett. 17,* 1905–1908 (1990).

Toon, G.C., C.B. Farmer, P.W. Schaper, L.L. Lowes, and R.H. Norton, Composition measurements of the 1989 Arctic winter stratosphere by airborne infrared solar absorption spectroscopy, *J. Geophys. Res. 97,* 7939–7961 (1992).

Toumi, R. and S. Bekki, The importance of the reactions between OH and ClO for stratospheric ozone, *Geophys. Res. Lett. 20,* 2447–2450 (1993).

Traub, W.A., K.V. Chance, D.G. Johnson, and K.W. Jucks, Stratospheric spectroscopy with the far-infrared spectrometer (FIRS-2): Overview and recent results, *S.P.I.E., 1491,* 298–307 (1991).

Traub, W.A., D.G. Johnson, and K.V. Chance, Stratospheric hydroperoxyl measurements, *Science 247,* 446–449 (1990).

Waters, J.W., J.C. Hardy, R.F. Jarnot, H.M. Pickett, and P. Zimmermann, A balloon-borne microwave limb sounder for stratospheric measurements, *J. Quant. Spectros. Radiat. Transfer 32,* 407–433 (1984).

Waters, J.W., R.A. Stachnik, J.C. Hardy, and R.F. Jarnot, ClO and O_3 stratospheric profiles: balloon microwave measurements, *Geophys. Res. Lett. 15,* 780–783 (1988).

Waters, J.W., L. Froidevaux, W.G. Read, G.L. Manney, L.S. Elson, D.A. Flower, R.F. Jarnot, and R.S. Harwood, Stratospheric ClO and ozone from the microwave limb sounder on the Upper Atmosphere Research Satellite, *Nature 362,* 597–602 (1993).

Webster, C.R., R.D. May, R. Toumi and J.A. Pyle, Active nitrogen partitioning and the nighttime formation of N_2O_5 in the stratosphere: Simultaneous in situ measurements of NO, NO_2, HNO_3, O_3, and N_2O using the BLISS diode laser spectrometer, *J. Geophys. Res. 95,* 13851–13866 (1990).

Wennberg, P.O., R.M. Stimpfle, E.M. Weinstock, A.E. Dessler, S.A. Lloyd, L.B. Lapson, J.J. Schwab, and J.G. Anderson, Simultaneous, in situ measurements of OH and HO_2, O_3, and H_2O: A test of modeled stratospheric HO_x chemistry, *Geophys. Res. Lett. 17,*

1909–1912 (1990).

Wennberg, P. O., R. C. Cohen, R. M. Stimpfle, J. P. Koplow, J. G. Anderson, R. J. Salawitch, D. W. Fahey, E. L. Woodbridge, E. R. Keim, R. S. Gao, C. R. Webster, R. D. May, D. W. Toohey, L. M. Avallone, M. H. Proffitt, M. Loewenstein, J. R. Podolske, K. R. Chan, and S. C. Wofsy, Removal of stratospheric O_3 by radicals: In situ measurements of OH, HO_2, NO, NO_2, ClO, and BrO, *Science 266,* 398–404 (1994).

Woodbridge, E. L., J. W. Elkins, D. W. Fahey, L. E. Heidt, S. Solomon, T. J. Baring, T. M. Gilpin, W. H. Pollock, S. M. Schauffler, E. L. Atlas, M. Loewenstein, J. R. Podolske, C. R. Webster, R. D. May, J. M. Gilligan, S. A. Montzka, and R. J. Salawitch, Estimates of total organic and inorganic chlorine in the lower stratosphere from in situ measurements during AASE II, *J. Geophys. Res.,* in press, (1994).

World Meteorological Organization, Global Ozone Research and Monitoring Project Report No. 16, Atmospheric ozone 1985: Assessment of our understanding of the processes controlling its present distribution and change, Geneva (1986).

World Meteorological Organization, Report of the International Ozone Trends Panel 1988, Geneva (1989).

This manuscript was prepared with the AGU LaTeX macros v3.1.

Figure 1. Portions of a single limb-scan sequence (6 minutes of integration time per spectrum) for the best features of OH in the far infrared spectrum, the $F_1, 7/2 \leftarrow F_1, 5/2$ lines at 118 cm^{-1}. Spectral features are identified down to the FIRS-2 detection limit. The limb-scan sequence shown is from 26 September 1989, centered in time at 1128 MDT.

Figure 2. Measured and modeled OH and HO_2 concentrations versus solar zenith angle. The concentrations are taken from Table 2 and linearly interpolated to altitudes of 38, 32, 28, and 24 km.

Figure 3. FIRS-2 balloon measurements from 26-27 September 1989 and corresponding model calculations. (a) H_2O_2, (b) HNO_3, (c) NO_2.

Figure 4. FIRS-2 and BMLS balloon measurements from 26-27 September 1989 for Cl_y species and corresponding model calculations using varying branching ratios for the reactions of ClO with OH and HO_2 to produce HCl.

Figure 5. Comparisons of measured and modeled [HOCl]/[HCl] and [ClO]/[HCl] ratios, assuming various branching ratios of the reactions of ClO with OH and HO_2 to produce HCl. The measured ClO and HCl concentrations are interpolated onto the altitude grid of the model.

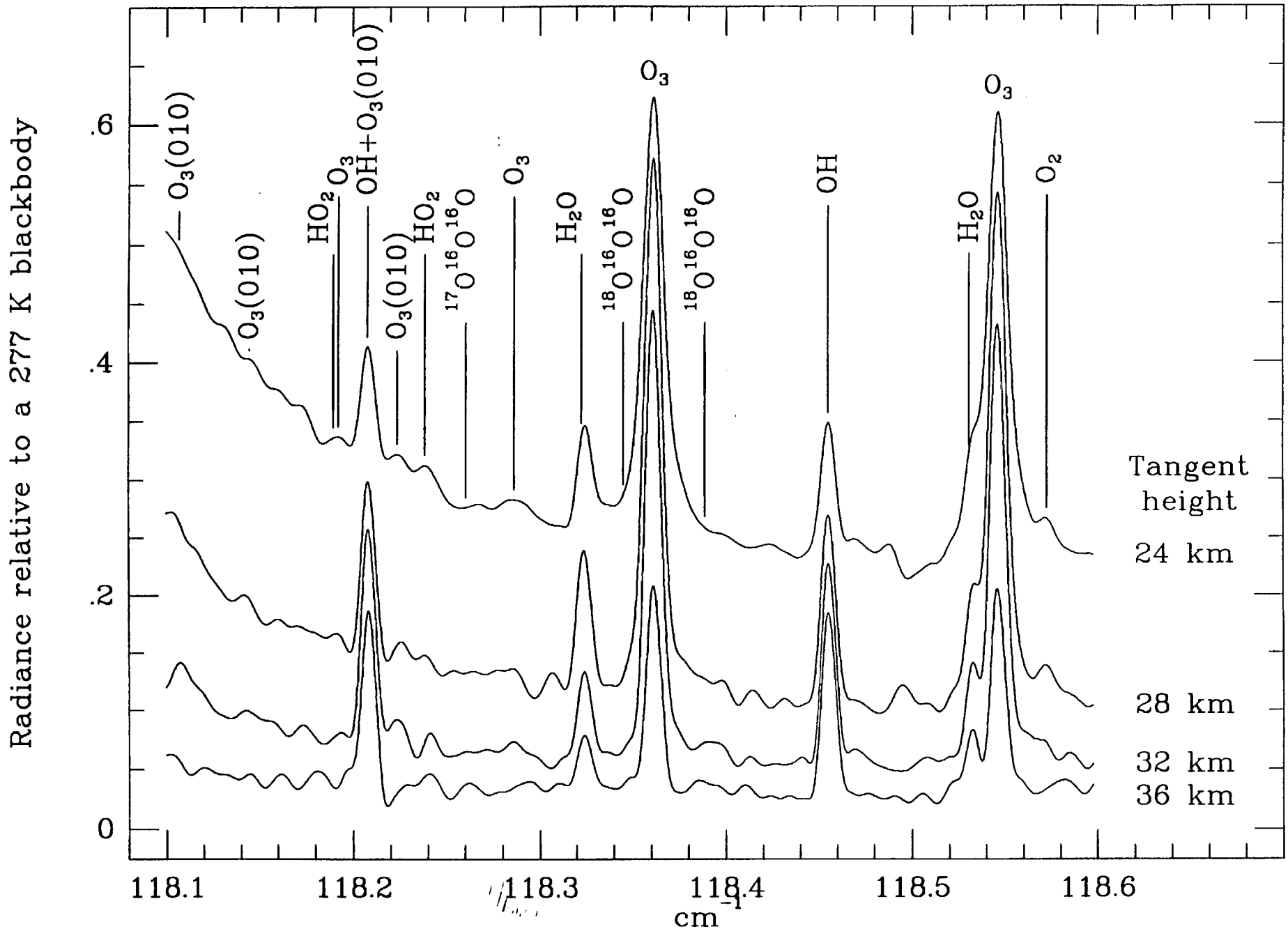
Radiance relative to a 277 K blackbody
.6
.4
.2
0
118.1
118.2
118.3
118.4
118.5
118.6
cm⁻¹
O3(010)
O3(010)
HO2
O3
OH+O3(010)
O3(010)
HO2
17O16O16O
O3
H2O
18O16O16O
O3
18O16O16O
OH
H2O
O3
O2
Tangent height
24 km
28 km
32 km
36 km

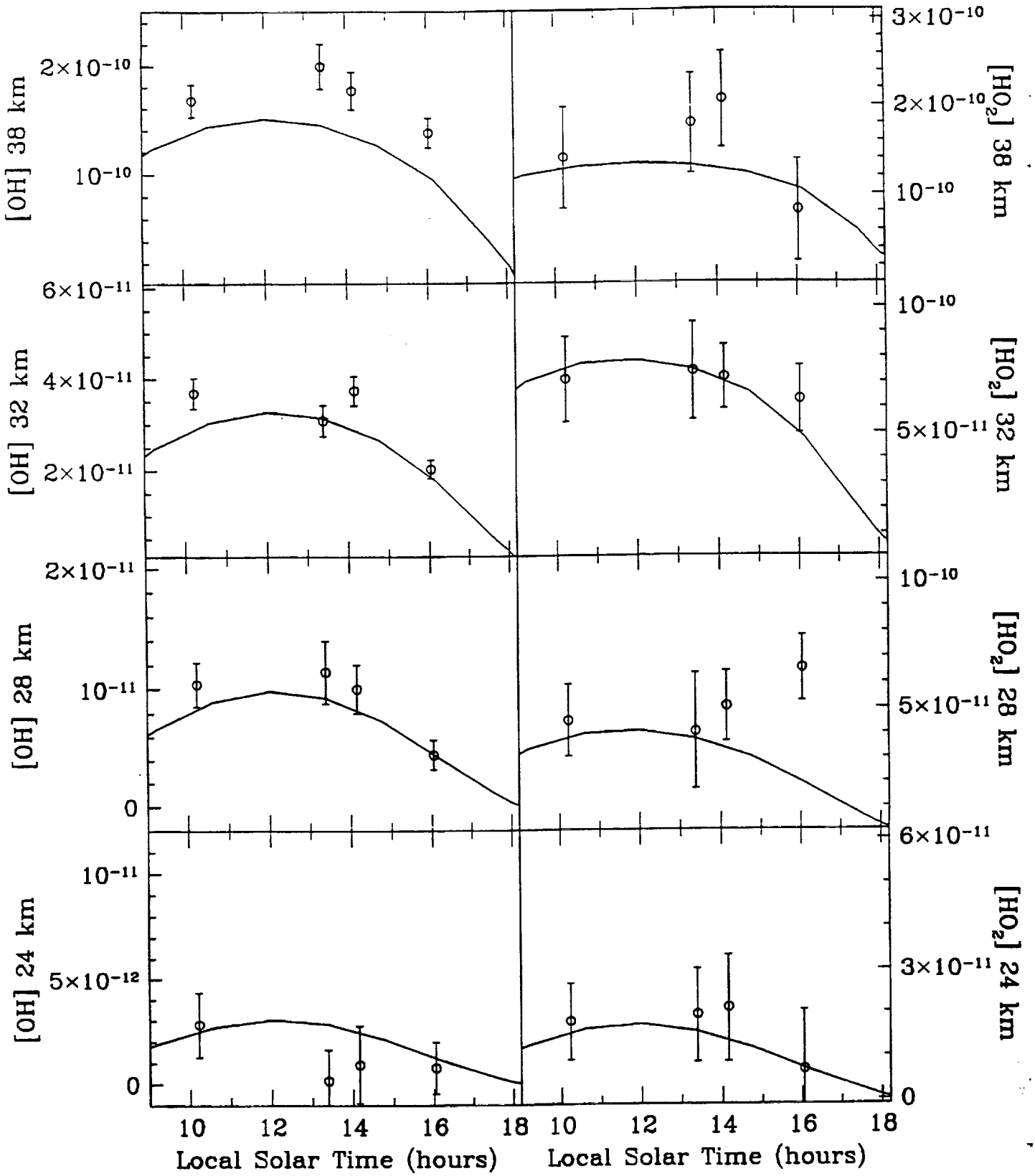
[OH] 38 km
2×10⁻¹⁰
10⁻¹⁰
6×10⁻¹¹
[HO₂] 38 km
3×10⁻¹⁰
2×10⁻¹⁰
10⁻¹⁰
[OH] 32 km
4×10⁻¹¹
2×10⁻¹¹
[HO₂] 32 km
10⁻¹⁰
5×10⁻¹¹
[OH] 28 km
2×10⁻¹¹
10⁻¹¹
0
[HO₂] 28 km
10⁻¹⁰
5×10⁻¹¹
[OH] 24 km
10⁻¹¹
5×10⁻¹²
0
[HO₂] 24 km
6×10⁻¹¹
3×10⁻¹¹
0
10 12 14 16 18
Local Solar Time (hours)
10 12 14 16 18
Local Solar Time (hours)

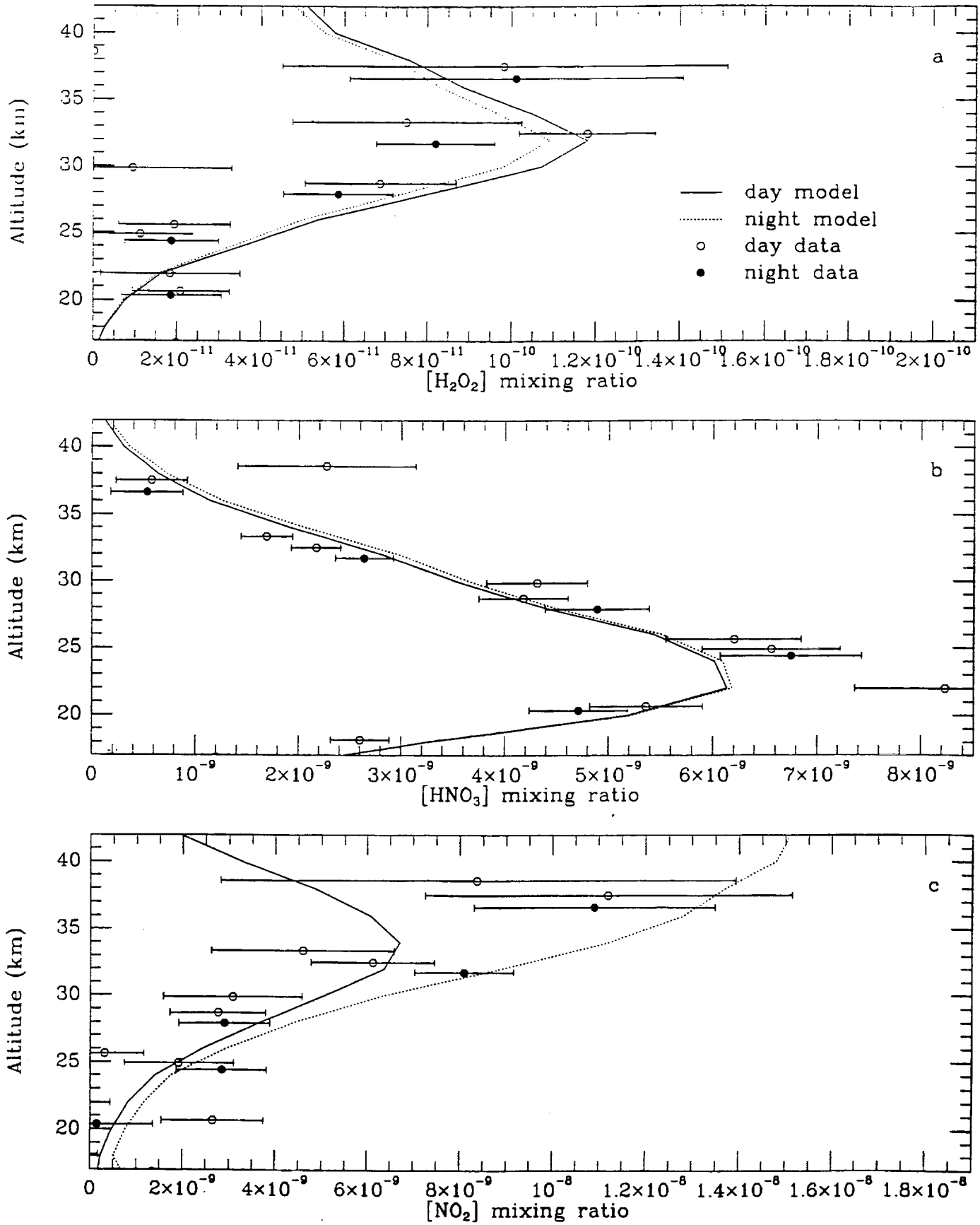
a
Altitude (km)
40
35
30
25
20
day model
night model
day data
night data
0
2×10⁻¹¹
4×10⁻¹¹
6×10⁻¹¹
8×10⁻¹¹
10⁻¹⁰
1.2×10⁻¹⁰
1.4×10⁻¹⁰
1.6×10⁻¹⁰
1.8×10⁻¹⁰
2×10⁻¹⁰
[H2O2] mixing ratio
b
Altitude (km)
40
35
30
25
20
0
10⁻⁹
2×10⁻⁹
3×10⁻⁹
4×10⁻⁹
5×10⁻⁹
6×10⁻⁹
7×10⁻⁹
8×10⁻⁹
[HNO3] mixing ratio
c
Altitude (km)
40
35
30
25
20
0
2×10⁻⁹
4×10⁻⁹
6×10⁻⁹
8×10⁻⁹
10⁻⁸
1.2×10⁻⁸
1.4×10⁻⁸
1.6×10⁻⁸
1.8×10⁻⁸
[NO2] mixing ratio

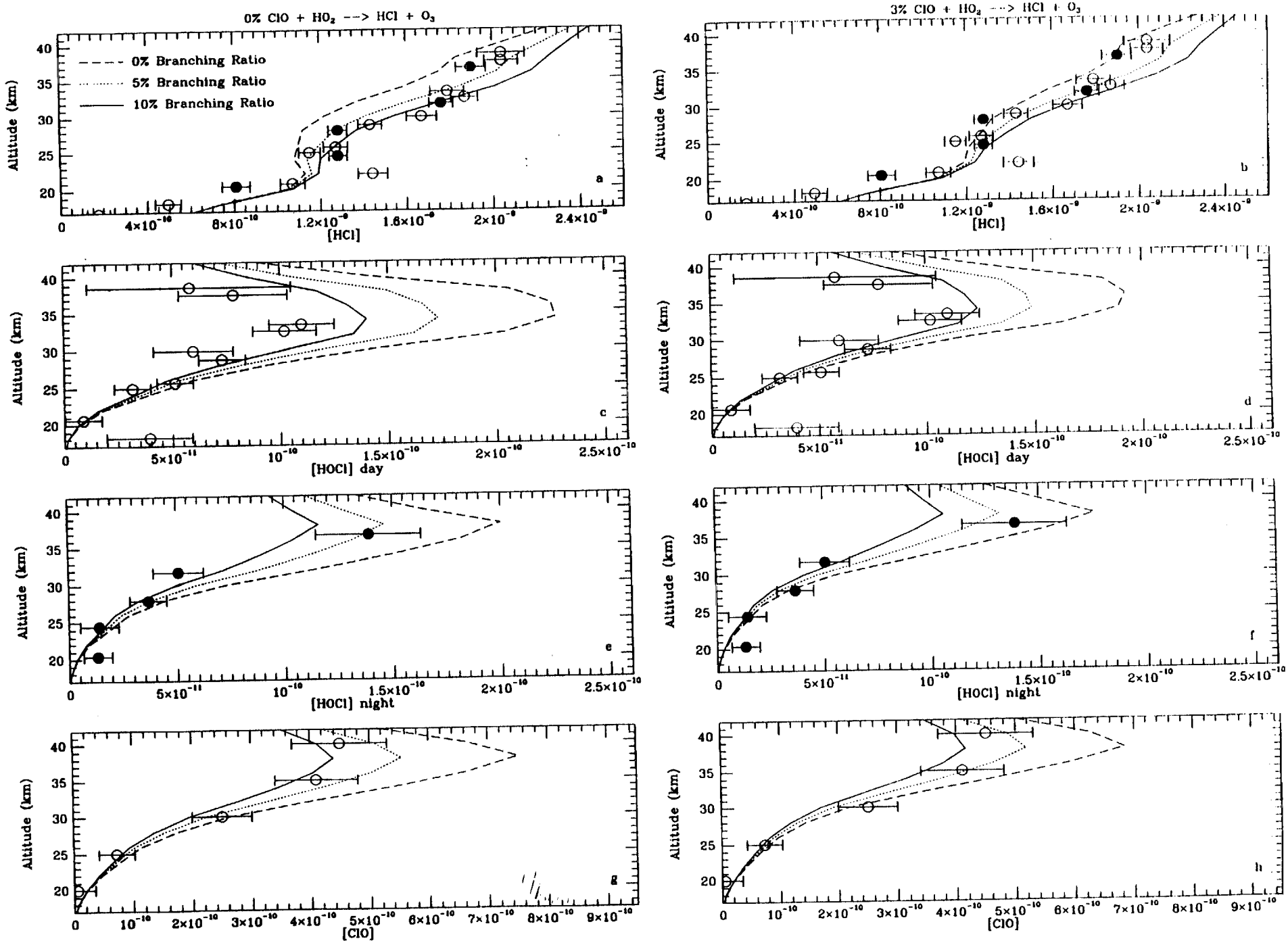
0% ClO + HO2 --> HCl + O3
0% Branching Ratio
5% Branching Ratio
10% Branching Ratio
Altitude (km)
[HCl]
a
3% ClO + HO2 --> HCl + O3
b
[HOCl] day
c
d
[HOCl] night
e
f
[ClO]
g
h

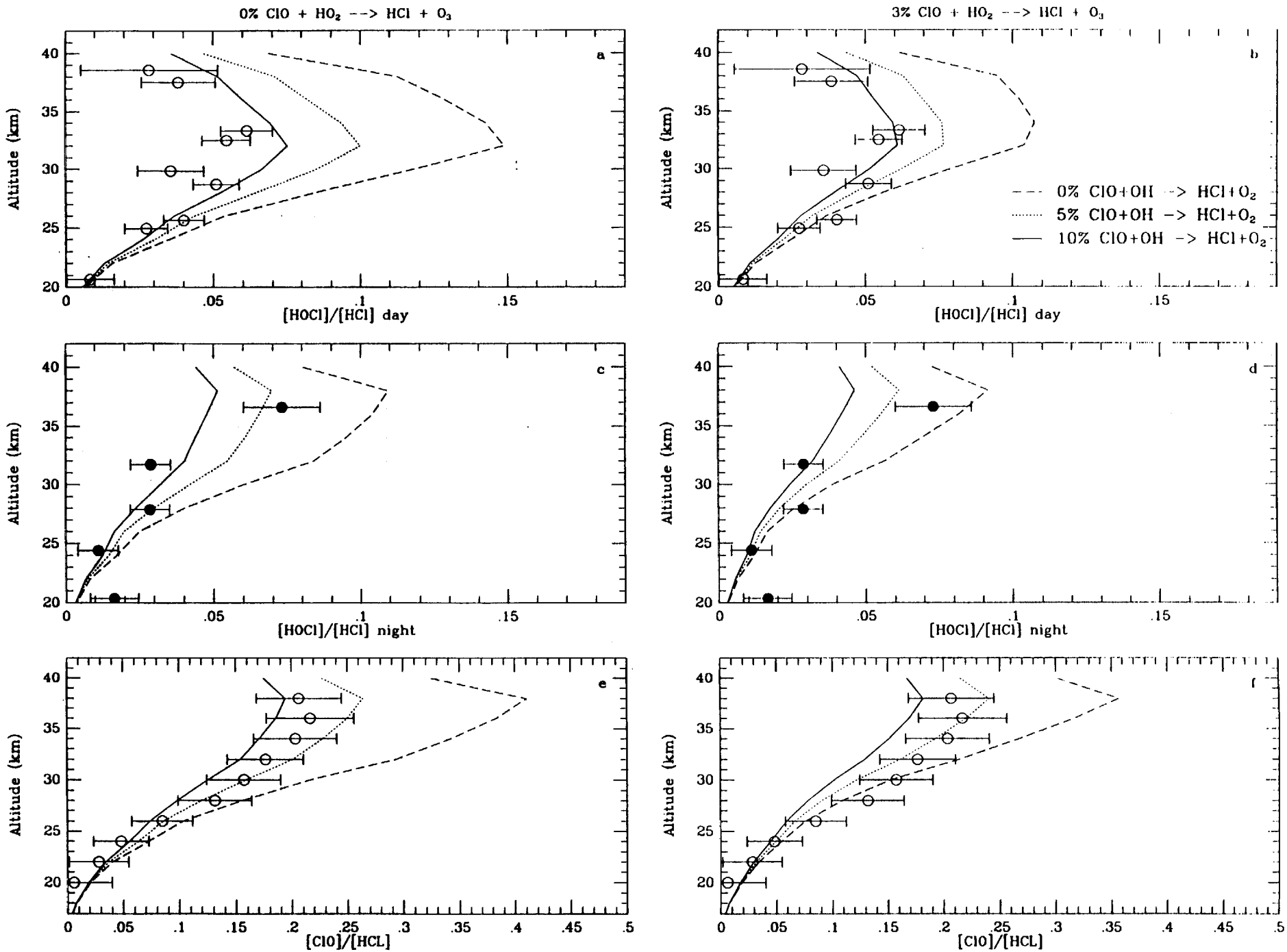
0% ClO + HO2 --> HCl + O3
3% ClO + HO2 --> HCl + O3
a
b
c
d
e
f
Altitude (km)
[HOCl]/[HCl] day
[HOCl]/[HCl] night
[ClO]/[HCL]
0% ClO+OH -> HCl+O2
5% ClO+OH -> HCl+O2
10% ClO+OH -> HCl+O2

Table 1. Retrieved FIRS-2 mixing ratio profiles

z (km)	Mixing ratios[a] H_2O (10^{-6})	H_2O_2 (10^{-12})	O_3 (10^{-6})	HNO_3 (10^{-9})	N_2O (10^{-8})	NO_2 (10^{-9})	HCl (10^{-9})	HOCl (10^{-11})
			26 September 1989 (9 limb scans, 1105-1818 MDT, SZA=51.4°)					
37.51	5.25(0.42)	98.1(53.0)	7.16(0.42)	0.58(0.35)	3.72(0.42)	14.3(3.47)	2.04(0.18)	7.83(2.52)
32.49	5.48(0.38)	118.(16.2)	8.71(0.46)	2.17(0.24)	8.68(0.79)	6.14(1.33)	1.87(0.16)	10.2(1.47)
28.71	4.66(0.33)	68.7(18.1)	7.47(0.41)	4.18(0.43)	14.5(1.30)	2.66(1.03)	1.43(0.13)	7.30(1.07)
24.91	4.17(0.37)	11.2(12.5)	4.24(0.25)	6.56(0.66)	19.1(1.65)	1.80(1.17)	1.15(0.10)	3.16(0.82)
20.66	4.18(0.38)	20.9(11.6)	3.06(0.25)	5.37(0.54)	21.1(1.78)	2.48(1.08)	1.07(0.10)	0.89(0.87)
16.84	1.85(0.50)	19.9(151.)	0.79(1.51)	1.20(0.13)	29.5(2.52)	7.48(17.2)	0.18(0.06)	−0.2(4.08)
			26-27 September 1989 (13 limb scans, 2028-0337 MDT, night measurement)					
36.63	5.06(0.35)	101.(39.7)	7.28(0.42)	0.53(0.35)	4.12(0.45)	10.9(2.59)	1.90(0.17)	13.9(2.42)
31.72	5.13(0.36)	81.9(14.1)	8.45(0.44)	2.64(0.28)	9.22(0.84)	8.10(1.06)	1.76(0.15)	5.08(1.17)
27.91	4.75(0.32)	58.6(13.2)	6.73(0.37)	4.89(0.50)	15.1(1.35)	2.90(0.98)	1.28(0.11)	3.67(0.84)
24.40	4.91(0.34)	18.7(11.2)	5.21(0.30)	6.75(0.68)	18.7(1.36)	2.84(0.98)	1.28(0.11)	1.42(0.88)
20.36	3.47(0.36)	18.6(11.9)	1.78(0.21)	4.71(0.47)	22.4(1.88)	0.15(1.21)	0.81(0.09)	1.33(0.65)
15.96	2.30(0.60)	61.1(333.)	0.22(1.44)	0.64(0.07)	28.3(2.39)	-	0.07(0.05)	3.17(7.44)
			27 September 1989 (3 limb scans, 1011-1235 MDT, SZA=43.5°)					
38.57	5.23(0.77)	-	7.14(0.52)	2.27(0.87)	1.97(0.53)	13.9(5.40)	2.04(0.20)	5.81(4.70)
33.34	5.53(0.46)	75.0(27.4)	8.04(0.49)	1.69(0.25)	6.98(0.72)	4.69(1.98)	1.79(0.16)	11.0(1.50)
29.87	5.21(0.41)	9.32(23.6)	7.94(0.48)	4.31(0.49)	10.6(1.10)	2.93(1.55)	1.67(0.15)	5.97(1.84)
25.63	4.71(0.35)	19.3(13.3)	5.42(0.33)	6.20(0.65)	12.2(1.17)	0.26(0.84)	1.27(0.12)	5.11(0.83)
21.96	4.50(0.39)	18.4(16.6)	2.47(0.25)	8.23(0.86)	16.6(1.56)	−1.0(1.59)	1.44(0.13)	−2.7(1.19)
18.14	4.06(0.55)	-	2.70(0.87)	2.60(0.29)	22.7(2.89)	−4.2(7.35)	0.49(0.07)	3.93(1.96)

[a] 1σ errors include uncertainties from molecular parameters:
H_2O (5%), H_2O_2 (2%), O_3 (5%), HNO_3 (10%), N_2O (8%), NO_2 (5%), HCl (8%), HOCl (3%).

Table 2. Time variation of OH and HO_2

Altitude (km)	Mixing ratio[a] OH (10^{-12})	HO_2 (10^{-11})
26 September 1989 1105–1324 MDT, SZA = 40°		
37.89	192.(22.0)	17.7(5.45)
32.78	34.8(3.92)	8.16(1.69)
29.17	16.6(3.07)	4.84(2.80)
25.22	−0.9(1.76)	2.16(1.18)
20.49	1.05(1.10)	1.33(0.81)
26 September 1989 1325–1559 MDT, SZA = 47°		
37.43	160.(16.3)	20.1(5.40)
32.23	42.1(4.02)	7.44(1.22)
28.19	12.7(2.20)	5.86(1.46)
24.16	2.24(1.59)	2.05(1.12)
21.15	3.62(2.46)	2.28(1.54)
26 September 1989 1600–1811 MDT, SZA = 67°		
37.08	98.1(9.85)	8.18(5.67)
33.16	20.9(2.27)	6.28(1.22)
28.14	4.59(1.29)	6.79(1.28)
24.59	0.74(1.23)	0.62(1.35)
20.55	0.88(1.19)	1.13(1.34)
27 September 1989 1011–1235 MDT, SZA = 44°		
38.57	183.(18.9)	15.0(6.23)
33.34	50.3(4.68)	7.41(1.49)
29.87	15.6(2.47)	6.68(2.02)
25.63	3.88(1.29)	1.76(0.69)
21.96	1.46(1.99)	1.86(1.12)

[a] 1σ errors include uncertainties from molecular parameters: OH(8%), HO_2 (2%).

Table 3. BMLS ClO mixing ratio profile

Altitude (km)	ClO mixing ratio[a] (10^{-12})
26 September 1989 1100–1600 MDT, SZA = 44°	
40.0	450.(80.)
35.0	410.(70.)
30.0	250.(50.)
25.0	73.(30.)
20.0	5.(30.)

[a] 1σ errors include uncertainties from molecular parameters.